Scaling of fault damage zones in carbonate rocks

Sylvain Mayolle, Roger Soliva, Yannick Caniven, Christopher Wibberley, Grégory Ballas, Gaétan Milesi, Stéphane Dominguez

Scaling of fault damage zones in carbonate rocks

Sylvain Mayolle[a*], Roger Soliva[a], Yannick Caniven[a], Christopher Wibberley[b], Gregory Ballas[a], Gaétan Milesi[a], Stephane Dominguez[a]

[a] Geosciences Montpellier, Université de Montpellier, Université des Antilles, CNRS, Rue du Truel 34095 Montpellier, France

[b] TOTAL EP, CSTJF, Av. Larribau 64018 Pau, France

Corresponding author:

*sylvain.mayolle@umontpellier.fr, Geosciences Montpellier, Batiment 22, Rue du Truel 34095 Montpellier, France, (33) 4 67 14 38 94 (S. Mayolle)

Key words: *fault damage; displacement; carbonates; scaling law; segmentation*

Abstract

A renewed interest in fault damage zones is aimed at better understanding stress perturbation around faults, earthquake ground motions and fluid flow in the upper crust. In this study, we analyse fault/fracture systems at the outcrop and map scale and define *displacement - thickness* (*D-T*) scaling of fault damage zones using scanlines, in carbonate rocks in France and Spain. We determine fault displacement and damage zone thickness perpendicular to fault planes and far from fault tips for 12 selected faults in four study sites. The data show a logarithmic decrease of fracture frequency from the fault cores. This decrease is characterized by local frequency peaks corresponding to variably-linked secondary fault segments and abandoned tips within the fault damage zone. *D-T* data comprised between 0 and 100 m of net fault displacement show a nearly linear scaling with very little scattering. Including two additional data for $D > 100$ m, the best fit corresponds better to a power law. We propose a new model based on fault segmentation and linkage to explain the linear scaling observed up to 100 m displacement, and we discuss the non-linear behaviour with respect to the role of mechanical layer thickness and the inhibition of the segmentation process down dip for large-scale faults.

1. Introduction

Deformed rock volumes in fault zones are usually classified as two distinct zones, the Core Zone (CZ) and the Damage Zone (DZ) (Shipton and Cowie, 2001; Billi et al., 2003; Kim et al., 2004; Berg and Skar, 2005). The core zone is generally characterised by the presence of fault rocks (e.g. Sibson, 2000; Fossen, 2016) with variable comminution degree and frequently well-developed cementation, generally acting as a barrier of permeability when the

fault is dormant. The damage zone develops through different processes such as initiation, propagation/interaction of faults or seismic ruptures (Cowie and Shipton, 1998; Peacock, 2001; Shipton and Cowie, 2003; Kim et al., 2004; Peacock et al., 2017). Depending on the nature of the deformed rock and the applied state of stress, a wide diversity of damage structures can be found such as tensile fractures, layer folding, stylolites, dilation, shear and compaction bands. These structures may produce significant and variable impacts on permeability anisotropy in and adjacent to faults and therefore on fault-related fluid flow (Chester and Logan, 1986; McGrath and Davison, 1995; Caine et al., 1996; Sibson, 2000; Jourde et al., 2002; Kim et al., 2004; Agosta et al., 2007; Faulkner et al., 2010; Ballas et al., 2015). Despite their importance for economic fluids, fault damage zone 3D structure, their scaling and flow properties remain poorly known and still debated.

The geometry of damage zones has been described, from map, outcrop and microstructural analyses (McGrath and Davison, 1995; Billi et al., 2003; Micarelli et al., 2003; Johansen and Fossen, 2008; Choi et al., 2016). The *Damage zone thickness* (*T*) is defined as the total adjacent rock volume on both sides of the fault core containing brittle damage structures related to the fault (Shipton and Cowie, 2001, 2003; Berg and Skar, 2005; Schueller et al., 2013; Choi et al., 2016). Many studies indicate that *T* seems to evolve with the net fault *Displacement (D)* (e.g, Evans, 1990; Knott et al., 1996; Shipton and Cowie, 2003; Manighetti et al., 2004; Mitchell and Faulkner, 2009, 2012; Faulkner et al., 2011; Savage and Brodsky, 2011; Torabi and Berg, 2011; Perrin et al., 2016) and some of them even reveal a proportional relationship between *T* and *D* for $D < 150$ m (Shipton and Cowie, 2003; Mitchell and Faulkner, 2009, 2012; Savage and Brodsky, 2011; Schueller et al., 2013). For $D > 150$ m, *T* seems to stabilize at a few hundred metres. However, despite this evidence for a *D-T* relationship and associated trends, the processes and mechanics causing this remain difficult to constrain because of the large scattering of data used, about two orders magnitude (Savage

and Brodsky, 2011). Many factors can be responsible for this scattering. Firstly, the methodologies used to measure or quantify *T* vary between studies with no systematic consensus. By combining many different published studies into a large scanline database, damage can be described by undifferentiated structures such as tensile fractures and deformation bands, whose frequency decreases with distance from the CZ (e.g. Chester and Logan, 1986; Beach et al., 1999; Schueller et al., 2013). Then, the external limit of the damage zone is defined as the point where the fracture frequency reaches the background fracture frequency value (Beach et al., 1999; Berg and Skar, 2005; Faulkner et al., 2006; de Joussineau et al., 2007; Mitchell and Faulkner, 2009) although background fracture frequency is usually difficult to determine, adding errors in the assessment of *T*. Secondly, the fault damage types (tip damage, wall damage, link damage) in the sense of Kim et al. (2004) or in the synthesis from Mitchell and Faulkner (2009) (also see Wilson et al., 2003; Blenkinsop, 2008), are not differentiated, probably also explaining a part of the *D-T* data scattering. Thirdly, differences in rock type could also produce a strong effect on fault zone architecture and potentially on the *D-T* scaling (e.g. Soliva et al., 2006; Roche et al., 2012; Ballas et al., 2014). Most of the studies whose aim is to characterize the *D-T* scaling law are mainly based on faults in siliciclastic lithologies (e.g. Knott et al., 1996; Fossen and Hesthammer, 2000; Du Bernard et al., 2002; Berg and Skar, 2005; de Joussineau and Aydin, 2007; Mitchell and Faulkner, 2009). Although carbonate fractured reservoirs are common and the understanding of fracture network complexity represents a major issue for exploration/production of georesources, the fault damage zones and their scaling properties are poorly constrained for this lithology (Micarelli et al., 2003; Micarelli et al., 2006; Balsamo et al., 2016; Maqbool et al., 2016).

In this paper, we focus on the analysis of fault damage in carbonate rocks. We first provide a map scale analysis of fault segmentation geometry and damage using analysis based on remote sensing orthophotos and outcrops. Secondly, we analyse small-scale fracture damage using scanlines adjacent to fault, cores far from fault tip zones, and on outcrops where displacement can be measured. This enabled the identification of 12 faults, on which we define the *D*-*T* relationship. We analyse the resulting scaling laws and discuss their properties with respect to the map scale observations and previous models proposed in the literature. Finally, we propose new explanations based on fault growth processes, and especially fault segmentation and linkage.

2. Geological setting

In this study, we focus on two areas located in the south of France (Languedoc) and close to the Eastern coast of Spain (Sant Mateu and Maestrat). These two sites show normal faults due to the Oligocene Mediterranean Sea opening and some reverse and strike-slip faults from the Paleogene Pyrenean orogeny contraction, all in Tethysian mudstone carbonates.

2.1 *Languedoc (south of France)*

The Languedoc region is located in the former western gulf of the Tethys Ocean (Fig. 1a). Most of the outcrops in the region contain marine sediments comprising stratified carbonate rocks (Fig. 1a). The Mesozoic sedimentary cover can reach a total thickness up to 3,000 m. In this study, the analysed faults only affect Jurassic and Cretaceous rocks. The Jurassic section is characterized by sublithographic marine limestones and is several hundred metres thick.

The Cretaceous rocks are characterized by marl and massive limestone alternations with ammonites and brachiopods fossils.

The Mesozoic cover was affected by Pyrenean shortening, expressed by three phases of deformation from Paleocene to Oligocene (Petit and Mattauer, 1995; Séranne et al., 1995; Benedicto et al., 1999). The first one is characterized by well-marked N020E-oriented fractures (Taha, 1986; Arthaud and Laurent, 1995), and kinematically consistent thrust faults. A second N145E oriented contraction is marked by N055E stylolites and N145E joints. A last N-S contractional stage is visible with N-S joints and E-W stylolites. This last contraction allows activation of the N020E joints and N055E stylolites in sinistral strike-slip (Petit et al., 1999; Soliva et al., 2010). These faults have also been reactivated during the Oligocene extension phase as normal faults (e.g. Arthaud and Mattauer, 1969).

Depending on the different accessibilities and outcrop quality in Languedoc area, this study focuses on the St Clement normal fault, the Taurac reverse fault and two other minor faults in the St Clement area. Like the crustal-scale Cevennes and Nimes faults, the St Clement fault was probably active during 3 tectonic phases. (1) NW-SE middle Cretaceous extension showing a normal phase of slip; (2) during the Paleocene to Eocene Pyrenean shortening, a sinistral strike-slip phase; and (3) a main phase during Oligocene NW-SE Gulf Lion rifting with around 550 m displacement on the fault (Arthaud and Mattauer, 1969; Steer et al., 2011). The brittles structures are mainly consistent with normal faulting, but a minority can be related to strike-slip events (Auzende et al., 1973; Séranne et al., 1995; Benedicto et al., 1999; Steer et al., 2011). The Taurac fault is a reverse strike-slip fault connected to the Cevennes fault. Striations on the main fault slip surface show reverse strike-slip and dip-slip reverse displacement.

2.2 *Maestrat*

The second study area is located at the eastern border of the Maestrat basin (Fig. 1b). The Maestrat is a part of the Iberian Range, which contains several kilometres of Mesozoic and Cenozoic sediments (Nebot Miralles and Guimerà i Rosso, 2016). This region was affected by two phases of extensional rifting with NW-SE trending normal faulting, from the Triassic to the mid-Cretaceous (Albian), during which time were deposited the Jurassic shallow carbonate platform, Cretaceous carbonates and different layers of marls (Salas and Casas, 1993; Salas et al., 2001, 2011; Martín-Martín et al., 2013). During the Middle Eocene to Early Miocene, the Alpine orogeny affected the basin with a contractional deformation (González, 1989).

A general tectonic extensional event followed the Alpine inversion, and caused the Catalan and Valencian coastal rifts. During Late Oligocene to Early Miocene this extensional stage generated multiple NE-SE minor normal faults through the Mesozoic carbonates (Roca and Guimerà, 1992; Salas and Casas, 1993; Salas et al., 2001). In the Sant Mateu area (Fig. 1b), the Mesozoic rocks are tilted 30° to the NE and the lithologies are consistent with Languedoc carbonates. In the Aliaga area the N-S Alpine inversion, during late Oligocene and early Miocene, generate strike slip fault and reverse faults with south and north vergence (Fig. 1b). Mesozoic cover rises to over 1,000 m altitude, being tilted and folded (Nebot Miralles and Guimerà i Rosso, 2016). In this area, there is no evidence of Neogene extensional reactivation.

In summary, the Languedoc and Maestrat study areas show carbonate rocks that were deposited during the Tethys ocean opening and were deformed both during the Alpine contractional events, and the extensional rifting during the Late Oligocene to Early Miocene. In the Sant Mateu and St Clement areas, folding is gentle and there is no evidence of thrust faults in the vicinity of the area.

3. Methods

3.1 *Terminology of brittle damage structures*

In this study, discontinuous deformation of the carbonate rocks observed in the field are qualified by 4 different terms, joints, veins, stylolites, and faults, and are identified in the field depending on their geometric and kinematic properties (Fig. 2). The term joint refers to a Mode I fracture, from metric to decametric length, for millimetre to centimetre opening, not sealed or filled with druse calcite. Veins are defined as centimetric to metric Mode I fractures and always cemented with sparitic calcite. They can also be described as “tension gashes”. Veins and joints are generally oriented perpendicular to the minor-principal stress axis (Fossen, 2016). A generic usage of the term “fracture” refers to both joints and veins. Veins and joints that affect carbonates are frequently preferential surfaces for dissolution, depending on cementation. In this study, three scanlines were made to sample structures on an outcrop that has suffered significant dissolution. In these cases dissolution patterns on the rock surface have been counted as fractures. Stylolites are dissolution surfaces also known as solution seams or Mode –I structures in carbonate rocks (Toussaint et al., 2018). They are perpendicular to the major-principal stress axis and also to veins or a set of joints.

Faults are slip planes of mode II or III tips of metric to kilometric length, generally showing one or multiple slickensides with slickenlines. DZ can include secondary minor faults and slickensides with a certain width of fault rocks in their individual CZs. Secondary faults in DZs are always indicated on the scanline histograms.

3.2 *Scanline measurements*

Measurement of fracture damage was performed along scanlines across the damage zones. A scanline consists of the fracture frequency measurement per linear metre along a sampling line. This frequency is also referred to as the fracture density (P10) as the number of fracture intersections along a 1D scanline (Dershowitz, 1984; Bisdom et al., 2014). The sampling step (*W*s), the distance over which the number of fractures is counted, is adapted to the total scanline length (Ls). For $Ls < 5$ m, $Ws = 10$ cm; for $5 \leq Ls \leq 20$ m, $Ws = 50$ cm; for $Ls > 20$ m, $Ws = 1$ m. When $Ws < 1$ m, the frequency is normalized to be comparable with others dataset.

The scanline is oriented nearly perpendicular to the fault trace and starting at the boundary between the main CZ and the DZ. Moreover all the scanlines satisfy several other criteria including (1) the position of the outcrop far from the observed fault tips at the map scale (2) the outcrop must be large enough to reach the background fracturing, (3) the lithology must be similar through the entire scanline, and (4) the fault net displacement must be measurable. We selected 12 fault outcrops meeting all these criteria allowing measurement of fracture frequency along 12 scanlines noted S1 to S12. Two of these scanlines (S5 and S6) actually come from the same fault but were measured at different places and along different carbonate layers.

The fractures counted on the outcrops were those visible to the naked eye along scanlines, and several effects can generate "gaps" in the outcrop. The vegetation and outcrop degradation are the major sources of gaps. For the reverse Taurac fault, the scanline is positioned along the wall of an artificial tunnel and exposed to calcite precipitation and speleothems. These gaps are reported in the histograms of the scanlines as shaded areas, which represent a proportion of the scanline length ranging between 0% for the smallest faults (S1, S3, S7 and S10) up to 48% for the largest scanline (S2).

On the studied outcrops, dissolved fractures were counted separately from the sealed veins on the histograms. The number of dissolved fractures thus brings together different types of fractures, veins, joints, and sub-vertical stylolitic surfaces.

3.3 *Damage zone thickness*

The DZ thickness is estimated using the cumulative frequency curve (Berg and Skar, 2005; Choi et al., 2016). The gaps in frequency value are corrected by adding an average value of the two measurements before and after the gap. According to Berg and Skar (2005) and Choi et al. (2016), the DZ thickness is defined by the distance to the fault core corresponding to the inflection of the cumulative frequency curve. This inflection shows a stabilization of fracture density away from the fault defined as the background fracturing. Most of the scanlines have two inflections of the cumulative frequency curve. In this study, it is the farthest inflection from the fault that is retained as the DZ thickness. This inflection corresponds to the value where the cumulative frequency curve reaches the lowest slope gradient, which means a lower and homogenous fracture density. The distance between the first and the second inflection is considered as the half of the DZ thickness uncertainty.

The cumulative frequency curve used to define DZ thickness has several advantages (Choi et al., 2016), including (1) a better detection of outer boundaries of the DZ based on the intersection point of the cumulative frequency trends, (2) less influence of structural effects like secondary faults on the general decay, and (3) a correction of the gaps based on adjacent cumulative frequency gradient.

The apparent thickness defined along the scanlines is corrected as the real damage zone thickness (T) using the angle between the scanlines and fault dip (Fig. 3). For the scanlines acquired only on the footwall or the hangingwall, the DZ thickness value is doubled, as proposed by Savage and Brodsky (2011). This value is very close to the “Total fault zone

thickness" used in literature, which actually includes the CZ thickness. The core zone thickness could not be measured for all the faults, but its thickness generally correspond to values lower than one order of magnitude of the DZ thickness (e.g. Childs et al., 2009; Fossen, 2016), and is therefore smaller than the estimated error.

3.4 *Fault displacement*

The scanlines are always acquired on faults whose displacement is quantifiable. Displacement (or net slip, *D*, Fig. 3) is determined using both fault surface dip, slickenline orientation, layer dip and the offset between fault cutoff lines. In cases where slickenlines or fault surfaces were not observed in the field (4 faults, referred to S7, S9, S10 and S11), we used the average of fault dip and slickenline data measured in the considered studied fault system. To define the error bars, we consider a minimum and maximum value of displacement using +/- 30° for the pitch of the value measured on the outcrop, or the mean value used for faults without slickenlines.

3.5 *Fracture orientations*

On all the scanlines, fracture orientations were systematically recorded along the profile to characterize the fault damage fracture trends with respect to background fracturing. These measurements have been made to identify the orientation of each type of deformation structure exposed in Section 3.1, and to verify that fracture orientations are sub-parallel and consistent with the orientation of the main fault. Field measurements were conducted using mini-tablets and FieldMove Clino ©Copyright Midland Valley Exploration Ltd 2014. The data were regularly double-checked with a classical compass and clinometer to check the potential deviation of the mini-tablet measurements (Allmendinger et al., 2017; Novakova and Pavlis, 2017). The treatment of fault and fracture plane orientations and their representation

on a stereogram has been done with the software Stereonet, R. W. Allmendinger © 2006-2016. Because of the large amount of fracture data, and their planes often being vertical, we represent them as “rose diagrams”. The orientations have also been measured for the background fracturing between faults, along outcrops distributed between faults at map scale.

3.6 *Map scale analysis*

Brittle damage at the map scale was characterized from geological maps, orthophotos of 0.5 m pixel size (PNAO from Centro Nacional de Information Geografica, ORTHO HR® from IGN), measured in the field, and synthetized into the QGIS 2.18 software for precise interpretation of the structures in the study area (Fig. 4 and A1). The main brittle faults being characterized by Earth surface objects (reliefs, shadows, layer and rock discontinuities, limits and lineaments in the vegetal cover), fault mapping is mainly derived from orthophoto lineaments (Clark and Wilson, 1994). A manual lineament interpretation approach allowed geological and anthropic lineaments to be distinguished. In many cases, vegetation, Quaternary sediments and anthropic cover provide significant censoring biases for more than 50% of the studied areas. This particularly affects the detection of small lineaments lower than 100 m in length, such as small faults and all Mode I fractures, that cannot be detected with such a method. To characterize Mode I and stylolite background fracturing at this map scale, we measured their orientation and density along 47 outcropping stations between faults.

4. Damage Zone analysis

4.1 *Map scale analysis*

The St Clement and Sant Mateu study areas allow the map-scale analysis of master fault geometry and the spatial distribution of secondary faults only (Fig. 4 and A1). The master fault observed on the West side of the Sant Mateu area is shown in Fig.4a. This master fault is formed of fault segments, with variable degrees of interaction (open relays, e.g. at Salzadella, Fig. 4b, or linked relays). The uplifted eastern side of this master fault exhibits many unlinked, adjacent secondary-fault segments. These secondary fault segments define a zone of brittle faulting adjacent to the master fault, which increases towards the northern fault tip. This type of secondary fault tip damage pattern at a smaller scale is also observed with small lineaments (Fig.4b). Note however that truncation and censoring biases are too large at this scale to correctly analyse fault damage patterns close to the secondary faults. In the St Clement area, the master fault is also composed of more or less linked fault segments (Fig. A1). Secondary fault patterns are observed close to the master fault tips, but also at its centre around a linked relay composed of two master fault segments.

Outcrop data show Mode I fracture mainly trending N030E to N060E, which is consistent with the main lineament orientations, secondary faults and the master fault (Fig. 4c). In St Clement, both fracture and lineament orientations are more scattered, between N030E and N090E, and that fracture orientations are more perturbed in relay zones at both sites. Fracture densities counted in these outcrops between faults allows a characterization of background fracturing, giving a P10 density ranging between 15 and 17 Mode I fracture/m.

4.2 *Scanline analysis*

In this section, we present the data of 12 scanlines (S1 to S12, Fig. 5), taken from 11 different faults. A total of more than 14,800 fractures were counted on all the scanlines. The

307 S1, S2, S3 and S4 scanlines (Fig. 5a, b, c and d) were acquired in the Languedoc region
308 (France); the S5, S6, S7, S8 and S9 (Fig. 5e, f, g, h and i) scanlines were acquired in the Sant
309 Mateu area (Spain) and S10, S11, S12 (Fig. 5j, k, l) were acquired in the Aliaga area (Spain).
310 Scanline S8 illustrates the decrease of damage decay with distance from a normal fault
311 oriented N097E 67°S, with a slickenline of 70°SW pitch (Fig. 6). Its displacement is
312 estimated at 27 m. The number of sealed fractures clearly shows a decrease along the profile
313 away from the main fault. As for scanline S8 (Fig. 5h and Fig. 6), all the scanlines show a
314 decrease in the frequency of sealed veins with increasing distance (Fig. 5). This decay can
315 have different shapes and can be distributed along the entire scanline, or localised close to the
316 main fault. The decay of fractures in S8 is not continuous, with a polymodal shape marked by
317 fracture frequency peaks present in both the inner and the outer damage zone. These peaks
318 systematically correspond to secondary faults observed at the outcrop. When the displacement
319 is greater than 50 m, the faults are often accompanied by minor faults in the damage zone of
320 the main fault (S2, S4, S6, S9, and S12 see Fig. 5b, d, f, g, and l). These minor faults have
321 small displacements, i.e. centimetric to metric. These secondary faults are always
322 accompanied by fractures frequency peaks, and can be the maximum of fracture density of the
323 entire scanline. Furthermore, when the displacement is lower than 50 m, several fractures
324 frequency peaks are present on the scanline. These peaks mark secondary fault initiation or tip
325 damage of another segment as in Fig. 2d. These secondary faults are observed at different
326 scales and dimensions, on scanlines (Fig. 5), in the field (Fig. 2d) or in map view (Fig. 4).
327 The stereograms representing fracture orientations by typology (Fig. 6c) show that the
328 veins and joints have on average the same orientation (N160E and N090E). In these
329 stereograms, as in each stereogram representing fractures without distinction of typology (Fig.
330 6), the most represented orientation is sub-parallel to the main fault, except close to the main
331 fault. The dip of these fractures is from 50 to 80° NW, also sub-parallel to the main fault.

On all the scanlines, stylolites do not show clear frequency decay, being of generally constant frequency overall along the scanline (except on S1 and S3). Along the S8 profile, two sets of stylolites are measured, (1) a sub-vertical set between 80° and 90° dip and nearly perpendicular to the fractures, and (2) a nearly horizontal set dipping 20° to 30° to the East, nearly parallel to the stratification. In the damage zones, we also observe fracture sets and stylolites with trends inconsistent with the Oligocene extension, revealing that a small proportion of the fractures, consistent with the absolute background fracture density, are present into the damage zones.

4.3 *D-T scaling law in carbonate rocks*

Fig. 7 shows *Damage zone thickness* and *Displacement* values estimated from the faults shown as scanlines in Fig. 5. The data acquired in the studied carbonate rocks clearly show a normal correlation between *T* and *D* on a log/log diagram (Fig. 7). They are continuous over three orders of magnitude of displacement and show little dispersion (Fig. 7).

The data fit to a power law of the type function in the form of:

$$y = Cx^{\alpha}$$

C being a constant and α the exponent, which is a real between 0 and 1 (Fig. 7a). The least square coefficient of the trend is R^2 = 0.93, in which α equals to 0.82, then very close to an affine relation, and *C* equals 1.6.

The function shows a good fit with the data from faults where D < 100 m. The *D-T* data follow a near-linear *D-T* law with a correlation coefficient of 0.97 (Fig. 7c and d). In contrast, in this part of the graph, literatures data are scattered over more than two orders magnitude (Fig. 8). Total damage zone thickness of St Clement (S4) and Taurac (S2) faults are clearly under the linear *D-T* scaling law. As these faults have displacements of 556 m and 516 m

357 respectively, this finding is coherent with the literature data and the *D-T* scaling law for
358 displacements over 150 m.
359
360

361 5. Discussion

362 The determination of the displacement and the DZ thickness based on 12 scanlines reveals
363 a well-defined *D-T* scaling relationship, characterised by a nearly-linear scaling over three
364 orders of magnitude of displacement and for displacement below 100 m. Over the value of
365 100 m displacement, the only two faults that can be measured define a bend in the scaling
366 relationship suggesting that DZ thickness may saturate around 150 m.
367

368 5.1 *Scattering in the D-T scaling*

369 Damage zone scaling relationships for faults with displacement lower than 100 m shows a
370 least square coefficient of $R^2 = 0.97$ with an exponent $\alpha = 0.95$, i.e. very close to a linear
371 scaling relationship. The accuracy of this data set contrasts with the scattering observed in the
372 Savage & Brodsky (2011) data compilation from various studies Fig. 8. Compared to this data
373 compilation, the data presented in Fig. 7 were acquired exclusively in non-porous carbonate
374 rocks, far from the fault tips and with the same methodology to estimate the DZ thickness. In
375 particular, the fact that scanlines have been acquired far from the fault tips, probably
376 contributes to reducing the scattering (Kim et al., 2004, Perrin et al., 2016). This suggests that
377 the spread of data observed in Savage & Brodsky (2011) can be due to several geological
378 factors and processes, including the rheology of the host rocks and the fault zone (Berg and
379 Skar, 2005; Fossen and Rotevatn, 2016; Philit et al., 2018), modalities of slip accumulation
380 (incremental ruptures, characteristic rupture size, creep; Hadizadeh and Law, 1991; Robert et

al., 1995; Gratier et al., 1999), but also to the method of determination of the damage thickness (Choi et al., 2016) and fault net slip.

In our approach, the method for determining fault displacement depends on both the offset of the layer and slickenline orientations measured in the field. The main source of error concerns the slip vector, and a quite large uncertainty has been considered in the error calculation (see Section 3.5). However that error bar for the displacement values is still generally lower than the error bars obtained for damage zone thicknesses (see Figs. 7 and 8). Although the error bar is quite large on damage zone thickness, the *D*-*T* values are much less scattered than the data provided by previous studies (Fig. 8). This is probably due to an improved consistency in the criteria chosen to measure fault damage and (Section 3.2), and a more restricted set of geological variables (e.g. same lithology).

Despite working in the same lithology and the same methodology, damage thickness values include some errors and uncertainties related to outcrop quality and therefore damage zone thickness determination. In some of the scanlines, outcrop comprises gaps due to weathering and vegetal cover, potentially affecting the trend in frequency decay. The determination of the damage zone thickness is less robust for large faults where the gaps can represent, in the worst case, 48% of the scan-line. In our study, for large faults such as S2 and S6, the DZ thickness might be underestimated due to the lack of outcrop continuity, or especially for S4 and S2, due to the scanline size which appears insufficient in length. Faults S4 and S2 are actually within the scale range of fault displacement at which the linearity of *D*-*T* scaling is generally considered lost and critically discussed in terms of data scattering (Savage and Brodsky, 2011; Mitchell and Faulkner, 2012) (Fig. 8). For these two faults, the mean fracture density observed at the end of the scanline is around 20 and 23 fractures/m, which close to the background fracture density measured far from the faults (15 fractures/m)

405 from the map scale fracture analysis (see section 4.1, Fig. A1). This suggests that the
406 scanlines for these two faults are actually large enough to reach the background fracturing.
407

408 5.2 *Damage zone growth model*

409 *5.2.1 Segmentation and linear D-T scaling*

410 Several conceptual and numerical models have been proposed to account for the growth of
411 damage zones around faults, including processes of fault propagation, fault slip accumulation,
412 and subsequent fault and fracture coalescence (e.g. Shipton and Cowie, 2001; Manighetti et
413 al., 2004; Micarelli et al., 2006; Childs et al., 2009; Faulkner et al., 2011; Schueller et al.,
414 2013). With the exception of Shipton and Cowie (2003), these models fail to explain a normal
415 correlation between displacement and DZ thickness. The slip-patch model of Shipton and
416 Cowie (2003) relates fault damage growth to the quasi-static stress distributed around the
417 incremental ruptures (also possible for dynamic ruptures, Griffith et al., 2009), and to the way
418 the fault ruptures in different places during its growth history. Although very interesting, and
419 probably accounting for the damage zone growth of an isolated fault, this model does not
420 clearly account for the major and well-known process of fault growth by segment linkage
421 inherent to most, fault systems (e.g. Peacock and Sanderson, 1991; Mansfield and Cartwright,
422 1996; Cowie, 1998; Soliva and Benedicto, 2004).

423 Segment linkage appears to be a prominent process of fault growth within the development
424 of fault populations (e.g. Peacock, 2003, and references therein), including the fault systems
425 studied here, and the concept has also been used to explain the step-wise development of fault
426 core zones and overall fault zone thickness development in general (Wibberley et al., 2008;
427 Childs et al., 2009). It therefore has significant impact on fracture frequency decay around
428 fault and damage zone growth. In most of the scanlines Fig. 5, the logarithmic decay of
429 fracture frequency is actually formed through addition of smaller secondary peaks of fracture

430 frequency. These fracture clusters have modal values decreasing toward the outside edges of
431 the fault damage zone and are generally related to the presence of secondary faults. In other
432 words, fault damage zones are actually formed of secondary faults with their own damage,
433 and in this way the entire topic of the damage zone thickness definition is a multi-scale
434 phenomenon. Complementary observations of the fault architecture in the field (Fig. 2d) or at
435 the map scale (Fig. 4 and A1) show that these faults are always composed of multiple partially
436 or fully linked segments at different scales, for both out-of-plane and in-plane observations
437 (also see section 4.1). These faults, as many others in fault systems, are formed of linked
438 faults segments, with abandoned tips (e.g. Peacock and Sanderson, 1991) or aborted small
439 faults in the stress drop zone of the master through-going fault (e.g. Gupta and Scholz, 2000),
440 with their own small damage zones. Such geometries are commonly observed in fault systems
441 and are inherent to scale invariant 3D fault patterns having linear *Displacement – Length*
442 scaling and fractal fault size distribution (e.g. Scholz and Cowie, 1990; Dawers et al., 1993;
443 Cowie et al., 1995; Cladouhos and Marrett, 1996; Schlische et al., 1996; Cowie and Shipton,
444 1998).

445 Fault segment linkage has also been identified as a self-similar process in terms of fault
446 displacement and spacing at relay zones (Peacock, 2003; Soliva and Benedicto, 2004;
447 Acocella and Neri, 2005; Fig. 9b). On a broad range of scales (i.e. displacement ranging
448 between 10^{-3} m and 10^{3} m), two fault segments are generally linked for a value of
449 displacement close to the value of spacing between them (Soliva and Benedicto, 2004). This
450 process of linkage therefore allows both the accumulation of displacement and fault damage
451 thickness by incorporating (1) the secondary damages of the former segments, (2) abandoned
452 tips and (3) small faults (Fig. 9a and d). In other words, fault linkage allows the creation of a
453 master fault and incorporation of both types of damages, i.e. wall, tip and link damages of

454 former segments at its vicinity. If this process is scale invariant the thickness of fault damage
455 must increase proportionally with displacement as proposed in Fig. 9c.
456
457 *5.2.2 Non-linear D-T scaling*
458 Although debatable, the *D-T* data obtained on the two largest faults (Fig. 7 and 8) define a
459 trend consistent with those observed by Savage and Brodsky (2011) and Mitchell and
460 Faulkner (2012). In both of those studies, a *D-T* linear scaling is observed up to a scale of
461 displacement of 100 – 150 m whereas lower or no increase of DZ thickness is observed for
462 larger fault displacement (Fig. 8). This however contrasts with what Perrin et al. (2016) show
463 from map scale analysis of damage only formed of secondary faults, especially close to fault
464 tip, such as the "tip damage" in the terms of Kim et al. (2004), or "parent fault" in the terms of
465 Marchal et al. (1998). This might be because at a certain scale, fault damage defined by Mode
466 I fractures (or deformation bands) is limited and that fault damage might still be present in the
467 form of secondary faults, far enough from the master fault and therefore not considered in
468 scanline analyses. We tested this hypothesis by reporting a DZ thickness obtained from map
469 analysis of secondary faults around the main faults in the Sant Mateu and St Clément study
470 areas (see section 4.1, Fig. 4 and Fig. A1). We also added data from the Têt fault zone cutting
471 crystalline rocks in the Pyrenees (Taillefer et al., 2017), which was also examined using
472 scanline and map analysis. These new data obtained at this scale suggest that fault damage
473 due to Mode I fractures might scale very differently to fault damage derived from secondary
474 faults only. This might be particularly expressed close to the tip of master faults, where Mode
475 I fracture damage should decrease in thickness towards the tip of the master fault as
476 displacement decreases to zero, whereas tip damage observed for secondary faults increases
477 towards the master fault tip, and scales with fault length (Perrin et al., 2016; Fig. 9d and Fig.
478 10). The scanline method is however fully efficient to define and understand the scaling of

Mode I fracture damage and to plot together enough data. Mapping of Mode I fracture or deformation band damage around faults is rarely possible (e.g. Flodin, 2003; Davatzes et al., 2005; Shipton and Cowie, 2003) and generally biased.

Several solutions might be envisaged to explain a non-linear scaling of Mode I fracture damage. The first one was proposed by Ampuero and Mao (2017), on the basis that fracture damage mainly results from co-seismic events (Griffith, 2009 and Aben et al, 2016) and which extent is limited by the thickness of the brittle crust hosting earthquakes. Fault ruptures restricted to the brittle crust and related stress perturbations do not increase proportionally in length and height (also see Soliva et al., 2006) and therefore imply scale-dependent rupture and damage properties, or at least that the thickness of the brittle crust is an upper limit to scale independence. An additional model proposed here is based on the segmentation model exposed in Section 5.2.1. Faults with displacements larger than 100 m might have a lower fault tip reaching the brittle-ductile transition (Schlische et al., 1996; Nicol et al. 1996; Manighetti et al., 2001), and will not be able to link with new fault segments down dip (Fig. 10). This change in crustal rock behaviour prevents fault linkage, link damage processes and the accumulation of fault damage from former faults segments. This process must also favour normal and reverse fault weakening by asperity removal such as proposed by Childs et al. (2009), and therefore inhibits asperity damage processes for such faults (e.g. Mitchell and Faulkner, 2009). Other types of scale dependent behaviour were documented in fault system scaling laws (size distribution, *Displacement – Length*) where faults are restricted at the base of the crust or major layer discontinuities within the brittle crust, and where few or no faults are able to cut the underlying units due to (1) its specific behaviour, or (2) a limited amount of remote strain (Ackermann et al., 2001; Bohnenstiehl and Carbotte, 2001; Soliva and Schultz, 2008). In some cases, this process can happen at the scale of stratigraphic units (Soliva et al., 2006), at which non-linear damage scaling has also been observed (Micarelli et al., 2006).

Finally, an additional model of scale dependent fault damage could be considered given that a significant part of the fractures might form during the interseismic periods such as described by Robert et al. (1995). Carbonate rocks in particular express pressure solution processes, which generally form during these interseismic periods or during fault creep. Although the scanlines of Fig. 5 are not correctly oriented to count stylolites, they generally show their presence in the damage zones, with kinematically coherent orientations in relation to Mode I fractures. Their specific localisation close to fault cores documented by Benedicto and Schultz (2010) in carbonate rocks, suggests that a part of fault damage strain is due to slow deformation, although the proportion remains unclear. It is worth noting that, for strike slip fault, slow interseismic strain is distributed around faults following an arctangent function, with wavelength being related to the fault locking depth and therefore the brittle-ductile transition depth (Savage and Burford, 1973). This potentially provides an additional process to explain non-linear scaling of fracture damage, especially for strike-slip faults documented by Savage and Brodsky (2011) at large scale. Such a hypothesis currently suffers from lack of field data on interseismic fracture damage and definitions of the fault locking depth, if any. Other potential processes generating fault damage, such as Mode I fractures due to fault-related folding, are also hard to demonstrate from these field data due to the lack of layer dip variations in the examples studied.

6. Conclusions

We present new results about fault damage in carbonate rocks combining fault system analysis at map scale and *D-T* scaling, implying the following main results:

1) The scanlines obtained from field data show a clear logarithmic decrease of fracture frequency as distance increases from the main fault, with local frequency peaks in the damage zone corresponding to secondary faults.
2) Faults are formed of linked segments and abandoned tips in the fault damage zones thickness.
3) *D-T* data comprised between 0 and 100 m fault displacement show a nearly linear *D-T* scaling (power law with exponent of 0.95, with a least square coefficient R^2 = 0.97).
4) Including two additional data with D > 100 m, the best fit is a power law with an exponent of 0.82 and R^2 = 0.93. As suggested by previous studies on fault damage zones, damage thickness tends to saturate with increasing displacement larger than 100 m, and such an upper bound may be related to mechanical unit thickness.
5) These new data are discussed with respect to fault segmentation observed in the field. We propose a new model which explains *D-T* scaling by fault growth through segment linkage and damage zone thickness accumulation.
6) *D-T* scaling data of the largest faults, as well as data from the literature for different rock types, suggest that Mode I fracture damage might be scale dependent for $D > 100$ m. This is discussed in terms of inhibition of the down-dip segmentation process and asperity weakening for crustal scale faults able to cut the entire brittle crust.

Acknowledgements

This work summarizes the first phase of results of the DAMAGE project, funded by TOTAL (main sponsor) and Geoscience Montpellier. The authors would like to thank Bertrand Gauthier and Samuel Douillez for discussions and collaboration in the field, and Andrea Billi and anonymous reviewer for their positive remarks and improvements.

References

F.M. Aben, M.-L. Doan, T.M. Mitchell, R. Toussaint, T. Reuschl´e, M. Fondriest, J.-P. Gratier, and F. Renard. Dynamic fracturing by successive coseismic loadings leads to pulverization in active fault zones. Journal of Geophysical Research: Solid Earth , 121:1–23, 2016. doi: 10.1002/2015JB012542.

Ackermann, R.V., Schlische, R.W., Withjack, M.O., 2001. The geometric and statistical evolution of normal fault systems: an experimental study of the effects of mechanical layer thickness on scaling laws. Journal of Structural Geology 23, 1803–1819.

Acocella, V., Neri, M., 2005. Structural features of an active strike-slip fault on the sliding flank of Mt. Etna (Italy). Journal of Structural Geology 27, 343–355.

Agosta, F., Prasad, M., Aydin, A., 2007. Physical properties of carbonate fault rocks, fucino basin (Central Italy): implications for fault seal in platform carbonates. Geofluids 7, 19–32. https://doi.org/10.1111/j.1468-8123.2006.00158.x

Arthaud, F., Laurent, P., 1995. Contraintes, déformation et déplacement dans l avant-pays Nord-pyrénéen du Languedoc méditerranéen. Geodinamica Acta 8, 142–157.

Allmendinger, R.W., Siron, C.R., Scott, C.P., 2017. Structural data collection with mobile devices: Accuracy, redundancy, and best practices. Journal of Structural Geology 102, 98–112. https://doi.org/10.1016/j.jsg.2017.07.011

Ampuero, J.P., Mao, X., 2017. Upper Limit on Damage Zone Thickness Controlled by Seismogenic Depth. In: Thomas, M.Y., Mitchell, T.M., Bhat, H.S. (Eds.), Geophysical Monograph Series. John Wiley & Sons, Inc., Hoboken, NJ, USA, 243–253. https://doi.org/10.1002/9781119156895.ch13

Arthaud, F., Mattauer, M., 1969. Exemples de stylolites d'origine tectonique dans le Languedoc, leurs relations avec la tectonique cassante. Bulletin de La Société Géologique de France 7, 738–744.

Auzende, J.M., Bonnin, J., Olivet, J.L., 1973. The origin of the western Mediterranean basin. Journal of the Geological Society 129, 607–620. https://doi.org/10.1144/gsjgs.129.6.0607

Ballas, G., Fossen, H., Soliva, R., 2015. Factors controlling permeability of cataclastic deformation bands and faults in porous sandstone reservoirs. Journal of Structural Geology 76, 1–21. https://doi.org/10.1016/j.jsg.2015.03.013

Ballas, G., Soliva, R., Benedicto, A., Sizun, J.-P., 2014. Control of tectonic setting and large-scale faults on the basin-scale distribution of deformation bands in porous sandstone (Provence, France). Marine and Petroleum Geology 55, 142–159. https://doi.org/10.1016/j.marpetgeo.2013.12.020

Balsamo, F., Clemenzi, L., Storti, F., Mozafari, M., Solum, J., Swennen, R., Taberner, C., Tueckmantel, C., 2016. Anatomy and paleofluid evolution of laterally restricted extensional fault zones in the Jabal Qusaybah anticline, Salakh arch, Oman. Geological Society of America Bulletin 128, 957–972. https://doi.org/10.1130/B31317.1

Beach, A., Welbon, A.I., Brockbank, P.J., McCallum, J.E., 1999. Reservoir damage around faults; outcrop examples from the Suez Rift. Petroleum Geoscience 5, 109–116. https://doi.org/10.1144/petgeo.5.2.109

Benedicto, A., Séguret, M., Labaume, P., 1999. Interaction between faulting, drainage and sedimentation in extensional hanging-wall syncline basins: Example of the Oligocene Matelles basin (Gulf of Lion rifted margin, SE France). Geological Society, London, Special Publications 156, 81–108.

603 Benedicto, A., Schultz, R.A., 2010. Stylolites in limestone: Magnitude of contractional strain
604 accommodated and scaling relationships. Journal of Structural Geology 32, 1250–
605 1256. https://doi.org/10.1016/j.jsg.2009.04.020
606 Berg, S.S., Skar, T., 2005. Controls on damage zone asymmetry of a normal fault zone:
607 outcrop analyses of a segment of the Moab fault, SE Utah. Journal of Structural
608 Geology 27, 1803–1822. https://doi.org/10.1016/j.jsg.2005.04.012
609 Billi, A., Salvini, F., Storti, F., 2003. The damage zone-fault core transition in carbonate
610 rocks: implications for fault growth, structure and permeability. Journal of Structural
611 Geology 25, 1779–1794. https://doi.org/10.1016/S0191-8141(03)00037-3
612 Bisdom, K., Gauthier, B.D.M., Bertotti, G., Hardebol, N.J., 2014. Calibrating discrete
613 fracture-network models with a carbonate three-dimensional outcrop fracture network:
614 Implications for naturally fractured reservoir modeling. AAPG Bulletin 98, 1351–
615 1376. https://doi.org/10.1306/02031413060
616 Blenkinsop, T.G., 2008. Relationships between faults, extension fractures and veins, and
617 stress. Journal of Structural Geology 30, 622–632.
618 https://doi.org/10.1016/j.jsg.2008.01.008
619 Bohnenstiehl, D.R., Carbotte, S.M., 2001. Faulting patterns near 19 30′ S on the East Pacific
620 Rise: Fault formation and growth at a superfast spreading center. Geochemistry,
621 Geophysics, Geosystems 2.
622 Caine, J.S., Evans, J.P., Forster, C.B., 1996. Fault zone architecture and permeability
623 structure. Geology 24, 1025–1028.
624 Chester, F.M., Logan, J.M., 1986. Implications for mechanical properties of brittle faults from
625 observations of the Punchbowl fault zone, California. Pure and Applied Geophysics
626 124, 79–106.
627 Childs, C., Manzocchi, T., Walsh, J.J., Bonson, C.G., Nicol, A., Schöpfer, M.P.J., 2009. A
628 geometric model of fault zone and fault rock thickness variations. Journal of Structural
629 Geology 31, 117–127. https://doi.org/10.1016/j.jsg.2008.08.009
630 Choi, J.-H., Edwards, P., Ko, K., Kim, Y.-S., 2016. Definition and classification of fault
631 damage zones: A review and a new methodological approach. Earth-Science Reviews
632 152, 70–87. https://doi.org/10.1016/j.earscirev.2015.11.006
633 Cladouhos, T.T., Marrett, R., 1996. Are fault growth and linkage models consistent with
634 power-law distributions of fault lengths? Journal of Structural Geology 18, 281–293.
635 Clark, C.D., Wilson, C., 1994. Spatial analysis of lineaments. Comput. Geosci. 20, 1237–
636 1258. doi:10.1016/0098-3004(94)90073-6
637 Cowie, P.A., Sornette, D., Vanneste, C., 1995. Multifractal scaling properties of a growing
638 fault population. Geophysical Journal International 122, 457–469.
639 Cowie, P.A., Shipton, Z.K., 1998. Fault tip displacement gradients and process zone
640 dimensions. Journal of Structural Geology 20, 983–997. https://doi.org/0191-8141/98
641 Davatzes, N.C., Eichhubl, P., Aydin, A., 2005. Structural evolution of fault zones in
642 sandstone by multiple deformation mechanisms: Moab fault, southeast Utah.
643 Geological Society of America Bulletin 117, 135–148.
644 Dawers, N.H., Anders, M.H., Scholz, C.H., 1993. Growth of normal faults: Displacement-
645 length scaling. Geology 21, 1107–1110.
646 de Joussineau, G., Aydin, A., 2007. The evolution of the damage zone with fault growth in
647 sandstone and its multiscale characteristics. Journal of Geophysical Research 112.
648 https://doi.org/10.1029/2006JB004711
649 de Joussineau, G., Mutlu, O., Aydin, A., Pollard, D.D., 2007. Characterization of strike-slip
650 fault–splay relationships in sandstone. Journal of Structural Geology 29, 1831–1842.
651 https://doi.org/10.1016/j.jsg.2007.08.006
652 Dershowitz, W.S., 1984. Rock joint systems. Massachusetts Institute of Technology.

Du Bernard, X., Labaume, P., Darcel, C., Davy, P., Bour, O., 2002. Cataclastic slip band distribution in normal fault damage zones, Nubian sandstones, Suez rift. Journal of Geophysical Research: Solid Earth 107, ETG 6-1-ETG 6-12. https://doi.org/10.1029/2001JB000493

Evans, J.P., 1990. Thickness-displacement relationships for fault zones. Journal of Structural Geology 12, 1061–1065. https://doi.org/10.1016/0191-8141(90)90101-4

Faulkner, D.R., Jackson, C.A.L., Lunn, R.J., Schlische, R.W., Shipton, Z.K., Wibberley, C.A.J., Withjack, M.O., 2010. A review of recent developments concerning the structure, mechanics and fluid flow properties of fault zones. Journal of Structural Geology 32, 1557–1575. https://doi.org/10.1016/j.jsg.2010.06.009

Faulkner, D.R., Mitchell, T.M., Healy, D., Heap, M.J., 2006. Slip on "weak" faults by the rotation of regional stress in the fracture damage zone. Nature 444, 922–925. https://doi.org/10.1038/nature05353

Faulkner, D.R., Mitchell, T.M., Jensen, E., Cembrano, J., 2011. Scaling of fault damage zones with displacement and the implications for fault growth processes. Journal of Geophysical Research 116. https://doi.org/10.1029/2010JB007788

Flodin, E., 2003. Structural evolution, petrophysics, and large-scale permeability of faults in sandstone, Valley of Fire.

Fossen, H., 2016. Structural geology. Cambridge University Press.

Fossen, H., Hesthammer, J., 2000. Possible absence of small faults in the Gullfaks Field, northern North Sea: implications for downscaling of faults in some porous sandstones. Journal of Structural Geology 22, 851–863.

Fossen, H., Rotevatn, A., 2016. Fault linkage and relay structures in extensional settings—A review. Earth-Science Reviews 154, 14–28. https://doi.org/10.1016/j.earscirev.2015.11.014

González, Á., 1989. Análisis tectosedimentario del terciario del borde SE de la depresión del Ebro (sector bajoaragonés y cubetas ibéricas marginales.

Gratier, J.-P., Renard, F., Labaume, P., 1999. How pressure solution creep and fracturing processes interact in the upper crust to make it behave in both a brittle and viscous manner. Journal of Structural Geology 21, 1189–1197.

Griffith, W.A., Rosakis, A., Pollard, D.D., Ko, C.W., 2009. Dynamic rupture experiments elucidate tensile crack development during propagating earthquake ruptures. Geology 37, 795–798. https://doi.org/10.1130/G30064A.1

Gupta, A., Scholz, C.H., 2000. A model of normal fault interaction based on observations and theory. Journal of Structural Geology 22, 865–879.

Hadizadeh, J., Law, R.D., 1991. Water-weakening of sandstone and quartzite deformed at various stress and strain rates. International Journal of Rock Mechanics and Mining Sciences & Geomechanics Abstracts 28, 431–439. https://doi.org/10.1016/0148-9062(91)90081-V

Johansen, T.E.S., Fossen, H., 2008. Internal geometry of fault damage zones in interbedded siliciclastic sediments. Geological Society, London, Special Publications 299, 35–56. https://doi.org/10.1144/SP299.3

Jourde, H., Flodin, E.A., Aydin, A., Durlofsky, L.J., Wen, X.-H., 2002. Computing permeability of fault zones in eolian sandstone from outcrop measurements. AAPG Bulletin 86, 1187–1200.

Kim, Y.-S., Peacock, D.C.P., Sanderson, D.J., 2004. Fault damage zones. Journal of Structural Geology 26, 503–517. https://doi.org/10.1016/j.jsg.2003.08.002

Knott, S.D., Beach, A., Brockbank, P.J., Brown, J.L., McCallum, J.E., Welbon, A.I., 1996. Spatial and mechanical controls on normal fault populations. Journal of Structural Geology 18, 359–372.

Manighetti, I., King, G.C.P., Gaudemer, Y., Scholz, C.H., Doubre, C., 2001. Slip accumulation and lateral propagation of active normal faults in Afar. Journal of Geophysical Research: Solid Earth 106, 13667–13696.

Manighetti, I., King, G., Sammis, C.G., 2004. The role of off-fault damage in the evolution of normal faults. Earth and Planetary Science Letters 217, 399–408. https://doi.org/10.1016/S0012-821X(03)00601-0

Mansfield, C.S., Cartwright, J.A., 1996. High resolution fault displacement mapping from three-dimensional seismic data: evidence for dip linkage during fault growth. Journal of Structural Geology 18, 249–263. https://doi.org/10.1016/S0191-8141(96)80048-4

Maqbool, A.-R., Moustafa, A.R., Dowidar, H., Yousef, M., 2016. Architecture of fault damage zones of normal faults, Gebel Ataqa area, Gulf of Suez rift, Egypt. Marine and Petroleum Geology 77, 43–53. https://doi.org/10.1016/j.marpetgeo.2016.04.012

Marchal, D., Guiraud, M., Rives, T., Van Den Driessche, J., 1998. Space and time propagation processes of normal faults. Geological Society, London, Special Publications 147, 51–70.

Martín-Martín, J.D., Gomez-Rivas, E., Bover-Arnal, T., Travé, A., Salas, R., Moreno-Bedmar, J.A., Tomás, S., Corbella, M., Teixell, A., Vergés, J., Stafford, S.L., 2013. The Upper Aptian to Lower Albian syn-rift carbonate succession of the southern Maestrat Basin (Spain): Facies architecture and fault-controlled stratabound dolostones. Cretaceous Research 41, 217–236. https://doi.org/10.1016/j.cretres.2012.12.008

McGrath, A.G., Davison, I., 1995. Damage zone geometry around fault tips. Journal of Structural Geology 17, 1011–1024.

Micarelli, L., Benedicto, A., Wibberley, C.A.J., 2006. Structural evolution and permeability of normal fault zones in highly porous carbonate rocks. Journal of Structural Geology 28, 1214–1227. https://doi.org/10.1016/j.jsg.2006.03.036

Micarelli, L., Moretti, I., Daniel, J.M., 2003. Structural properties of rift-related normal faults: the case study of the Gulf of Corinth, Greece. Journal of Geodynamics 36, 275–303. https://doi.org/10.1016/S0264-3707(03)00051-6

Mitchell, T.M., Faulkner, D.R., 2012. Towards quantifying the matrix permeability of fault damage zones in low porosity rocks. Earth and Planetary Science Letters 339–340, 24–31. https://doi.org/10.1016/j.epsl.2012.05.014

Mitchell, T.M., Faulkner, D.R., 2009. The nature and origin of off-fault damage surrounding strike-slip fault zones with a wide range of displacements: A field study from the Atacama fault system, northern Chile. Journal of Structural Geology 31, 802–816. https://doi.org/10.1016/j.jsg.2009.05.002

Nebot Miralles, M., Guimerà i Rosso, J.J., 2016. Structure of an inverted basin from subsurface and field data. Geologica Acta 14, 0155–177.

Nicol, A., Watterson, J., Walsh, J.J., Childs, C., 1996. The shapes, major axis orientations and displacement patterns of fault surfaces. Journal of Structural Geology 18, 235–248.

Novakova, L., Pavlis, T.L., 2017. Assessment of the precision of smart phones and tablets for measurement of planar orientations: A case study. Journal of Structural Geology 97, 93–103. https://doi.org/10.1016/j.jsg.2017.02.015

Peacock, D.C.P., 2001. The temporal relationship between joints and faults. Journal of Structural Geology 23, 329–341.

Peacock, D.C.P., 2003. Scaling of transfer zones in the British Isles. Journal of Structural Geology 25, 1561–1567.

Peacock, D.C.P., Sanderson, D.J., 1991. Displacements, segment linkage and relay ramps in normal fault zones. Journal of Structural Geology 13, 721–733.

752 Peacock, D.C.P., Dimmen, V., Rotevatn, A., Sanderson, D.J., 2017. A broader classification
753 of damage zones. Journal of Structural Geology 102, 179–192.
754 https://doi.org/10.1016/j.jsg.2017.08.004
755 Perrin, C., Manighetti, I., Gaudemer, Y., 2016. Off-fault tip splay networks: A genetic and
756 generic property of faults indicative of their long-term propagation. Comptes Rendus
757 Geoscience 348, 52–60. https://doi.org/10.1016/j.crte.2015.05.002
758 Petit, J.-P., Mattauer, M., 1995. Palaeostress superimposition deduced from mesoscale
759 structures in limestone: the Matelles exposure, Languedoc, France. Journal of
760 Structural Geology 17, 245249–247256.
761 Petit, J.-P., Wibberley, C.A., Ruiz, G., 1999. Crack–seal', slip: a new fault valve mechanism?
762 Journal of Structural Geology 21, 1199–1207.
763 Philit, S., Soliva, R., Castilla, R., Ballas, G., Taillefer, A., 2018. Clusters of cataclastic
764 deformation bands in porous sandstones. Journal of Structural Geology 114, 235–250.
765 https://doi.org/10.1016/j.jsg.2018.04.013
766 Robert, F., Boullier, A.-M., Firdaous, K., 1995. Gold-quartz veins in metamorphic terranes
767 and their bearing on the role of fluids in faulting. Journal of Geophysical Research:
768 Solid Earth 100, 12861–12879. https://doi.org/10.1029/95JB00190
769 Roca, E., Guimerà, J., 1992. The Neogene structure of the eastern Iberian margin: Structural
770 constraints on the crustal evolution of the Valencia trough (western Mediterranean).
771 Tectonophysics 203, 203–218. https://doi.org/10.1016/0040-1951(92)90224-T
772 Roche, V., Homberg, C., Rocher, M., 2012. Architecture and growth of normal fault zones in
773 multilayer systems: A 3D field analysis in the South-Eastern Basin, France. Journal of
774 Structural Geology 37, 19–35. https://doi.org/10.1016/j.jsg.2012.02.005
775 Salas, R., Casas, A., 1993. Mesozoic extensional tectonics, stratigraphy and crustal evolution
776 during the Alpine cycle of the eastern Iberian basin. Tectonophysics 228, 33–55.
777 Salas, R., García-Senz, J., Guimerà, J., Bover-Arnal, T., 2011. Opening of the Atlantic and
778 development of the Iberian intraplate rift basins during the late Jurassic-early
779 Cretaceous. CM 2010-Abstracts 3, 245–248.
780 Salas, R., Guimerà, J., Mas, R., Martín-Closas, C., Meléndez, A., Alonso, A., 2001. Evolution
781 of the Mesozoic central Iberian Rift System and its Cainozoic inversion (Iberian
782 chain). Peri-Tethys Memoir 6, 145–185.
783 Savage, J.C., Burford, R.O., 1973. Geodetic determination of relative plate motion in central
784 California. Journal of Geophysical Research 78, 832–845.
785 Savage, H.M., Brodsky, E.E., 2011. Collateral damage: Evolution with displacement of
786 fracture distribution and secondary fault strands in fault damage zones. Journal of
787 Geophysical Research 116, 1–14. https://doi.org/10.1029/2010JB007665
788 Schlische, R.W., Young, S.S., Ackermann, R.V., Gupta, A., 1996. Geometry and scaling
789 relations of a population of very small rift-related normal faults. Geology 24, 683–686.
790 Scholz, C.H., Cowie, P.A., 1990. Determination of total strain from faulting using slip
791 measurements. Nature 346, 837.
792 Schueller, S., Braathen, A., Fossen, H., Tveranger, J., 2013. Spatial distribution of
793 deformation bands in damage zones of extensional faults in porous sandstones:
794 Statistical analysis of field data. Journal of Structural Geology 52, 148–162.
795 https://doi.org/10.1016/j.jsg.2013.03.013
796 Séranne, M., Benedicto, A., Labaum, P., Truffert, C., Pascal, G., 1995. Structural style and
797 evolution of the Gulf of Lion Oligo-Miocene rifting: Role of the Pyrenean orogeny.
798 Marine and Petroleum Geology 12, 809–820.
799 Shipton, Z.K., Cowie, P.A., 2003. A conceptual model for the origin of fault damage zone
800 structures in high-porosity sandstone. Journal of Structural Geology 25, 333–344.

Shipton, Z.K., Cowie, P.A., 2001. Damage zone and slip-surface evolution over μm to km scales in high-porosity Navajo sandstone, Utah. Journal of Structural Geology 23, 1825–1844.

Sibson, R.H., 2000. Fluid involvement in normal faulting. Journal of Geodynamics 29, 469–499.

Soliva, R., Benedicto, A., 2004. A linkage criterion for segmented normal faults. Journal of Structural Geology 26, 2251–2267. https://doi.org/10.1016/j.jsg.2004.06.008

Soliva, R., Benedicto, A., Maerten, L., 2006. Spacing and linkage of confined normal faults: Importance of mechanical thickness. Journal of Geophysical Research 111. https://doi.org/10.1029/2004JB003507

Soliva, R., and R. A. Schultz, 2008. Distributed and localized faulting in extensional settings : Insight from the North Ethiopian RiftAfar transition area, Tectonics, 27, TC2003, doi:10.1029/2007TC002148.

Soliva, R., Maerten, F., Petit, J.-P., Auzias, V., 2010. Field evidences for the role of static friction on fracture orientation in extensional relays along strike-slip faults: Comparison with photoelasticity and 3-D numerical modeling. Journal of Structural Geology 32, 1721–1731. https://doi.org/10.1016/j.jsg.2010.01.008

Steer, P., Bigot, A., Cattin, R., Soliva, R., 2011. In-situ characterization of the effective elasticity of a fault zone, and its relationship to fracture spacing. Journal of Structural Geology 33, 1541–1553. https://doi.org/10.1016/j.jsg.2011.09.009

Taha, M., 1986. Apport de la microtectonique cassante aux problemes des trajectoires de contraintes et de leurs perturbations (exemple du Nord de Montpellier).

Taillefer, A., Soliva, R., Guillou-Frottier, L., Le Goff, E., Martin, G., Seranne, M., 2017. Fault-Related Controls on Upward Hydrothermal Flow: An Integrated Geological Study of the Têt Fault System, Eastern Pyrénées (France). Geofluids 2017, 1–19. https://doi.org/10.1155/2017/8190109

Torabi, A., Berg, S.S., 2011. Scaling of fault attributes: A review. Marine and Petroleum Geology 28, 1444–1460. https://doi.org/10.1016/j.marpetgeo.2011.04.003

Toussaint, R., Aharonov, E., Koehn, D., Gratier, J.-P., Ebner, M., Baud, P., Rolland, A., Renard, F., 2018. Stylolites: A review. Journal of Structural Geology 114, 163–195. https://doi.org/10.1016/j.jsg.2018.05.003

Wibberley, C.A.J., Yielding, G., Di Toro, G., 2008. Recent advances in the understanding of fault zone internal structure: a review. Geological Society, London, Special Publications 299, 5–33. https://doi.org/10.1144/SP299.2

Wilson, J.., Chester, J.., Chester, F.., 2003. Microfracture analysis of fault growth and wear processes, Punchbowl Fault, San Andreas system, California. Journal of Structural Geology 25, 1855–1873. https://doi.org/10.1016/S0191-8141(03)00036-1

839 **Figures Captions**

840

841 **Fig. 1** Locations and geological schemes of the studied areas. a) Cenozoic cover map in
842 Languedoc area. Red box 1 is the St Clement fault study area. Red box 2 is the Taurac fault
843 study area. The regional stratigraphic column shows, in red, layers where damage
844 measurements are made in this study. Stereogram shows the average fracture and fault
845 orientations in these areas. Cross section according to the profile A-A'. b) Cenozoic cover
846 map in Maestrat study area. Red box 3 is the Sant Mateu study area and red box 4 is the
847 Aliaga study area. Similarly to a), the regional stratigraphic column, stereogram and cross
848 section according to profile B-B' are also represented for this area.

849

850

851 **Fig. 2** Brittle structures in carbonate rocks measured in the field. a) Joint sealed by sparite
852 mineralization. b) Tension crack Mode I opening sealed by sparite mineralization. c)
853 Horizontal stylolite associated with vertical fracture. d) Normal fault with 1.5 m displacement.
854 This fault has been selected for scanline measurement (Fig. 5a).

855

856

857 **Fig. 3** Scheme for the damage zone thickness correction using the angle between the
858 scanline and the normal to the fault plane.

859

860

861 **Fig. 4** Geological and mapping data in Sant mateu area. a) Sant Mateu master fault trace.
862 b) Geological map of the Sant Mateu area. Stereograms correspond to field fracture

863 measurements on one outcrop. c) Average orientation of the 1358 lineaments traces on map.
864 d) Colour chart for stereogram.
865
866
867 **Fig. 5** Total scanlines sampled in the four study areas. a), c), d) have been sampled in St
868 Clement, b) Taurac fault, e), f), g), h), i) at Sant Mateu and j), k), l) in Aliaga area. Yellow
869 dashed line marked the DZ boundary estimated with cumulative frequency curve. Faults with
870 0.5 m and 1 m displacement have only one inflection due to the small DZ thickness. Grey
871 boxes represent all the gaps where the outcrop quality prevents measurement.
872
873
874 **Fig. 6** Detail S8 scanline and average fractures orientations on normal fault in Sant Mateu.
875 a) Picture of the fault and the outcrop where the scanline was done (blue line). d) Scanline
876 histogram with fracture frequency as a function of the distance to the fault. The DZ thickness
877 (yellow dashed line) is determined by the inflection of the cumulative frequency curve (grey
878 dot). c) (up) Rose diagram of the fracture orientations classified in function of their types. The
879 length of each segment represents the proportional orientation for each fracture types. (down)
880 Rose diagram of unclassified fracture orientations, proportions of orientations are represented
881 independently to the fracture types.
882
883
884 **Fig. 7** Damage zone thickness data for this study as a function of displacement. Data show
885 an accurate linear law mainly define by normal faults, in carbonate rocks. a) log-log diagram
886 for all 12 scanlines, b) Same as a) with linear axis. The two faults with displacements over

100 m show significant deviation of the linear correlation. c) and d) Same as a) and b) without outliers (S2 and S4).

Fig. 8 Total fault zone thickness as a function of displacement modified from Savage and Brodsky, 2011. Linear scaling is well defined for faults displacement between 1 m and 100 m in carbonate rocks. Two faults over 100 m displacement seem to start the bending of the scaling law trend. Têt fault is a normal fault in Eastern Pyrénées, affecting granit and mylonite. Point with dot contour represent fault DZ evaluated in map view with secondary fault damage, for St Clement fault, Sant Mateu master faults and Têt fault (from Taillefer et al., 2017).

Fig. 9 Model of fault segmentation and damage zone growth. a) 3D model of segmented master fault with secondary faults and associated Mode I fracture damage zone. b) Spacing (S) between linking master faults as function of the displacement. c) Mode I damage zone increasing as function of the displacement and segment linkage show in d). d) Model of Mode I fracturing damage increased by fault segment linkage and tip secondary fault incorporation.

Fig. 10 a) Diagram for Mode I and secondary fault damage zone. b) Mode I damage zone growth by fault segments interaction. c) Fault segment linkage model inhibited by brittle ductile transition.

Appendices

912

913 **Fig. A1** Geological and mapping data in St Clement area. a) Geological map of the St
914 Clement area. Stereograms correspond to field fracture measurements on one outcrop. b)
915 Colour chart for stereogram. c) Average orientation of the 532 lineaments traces on map.

916

917

918

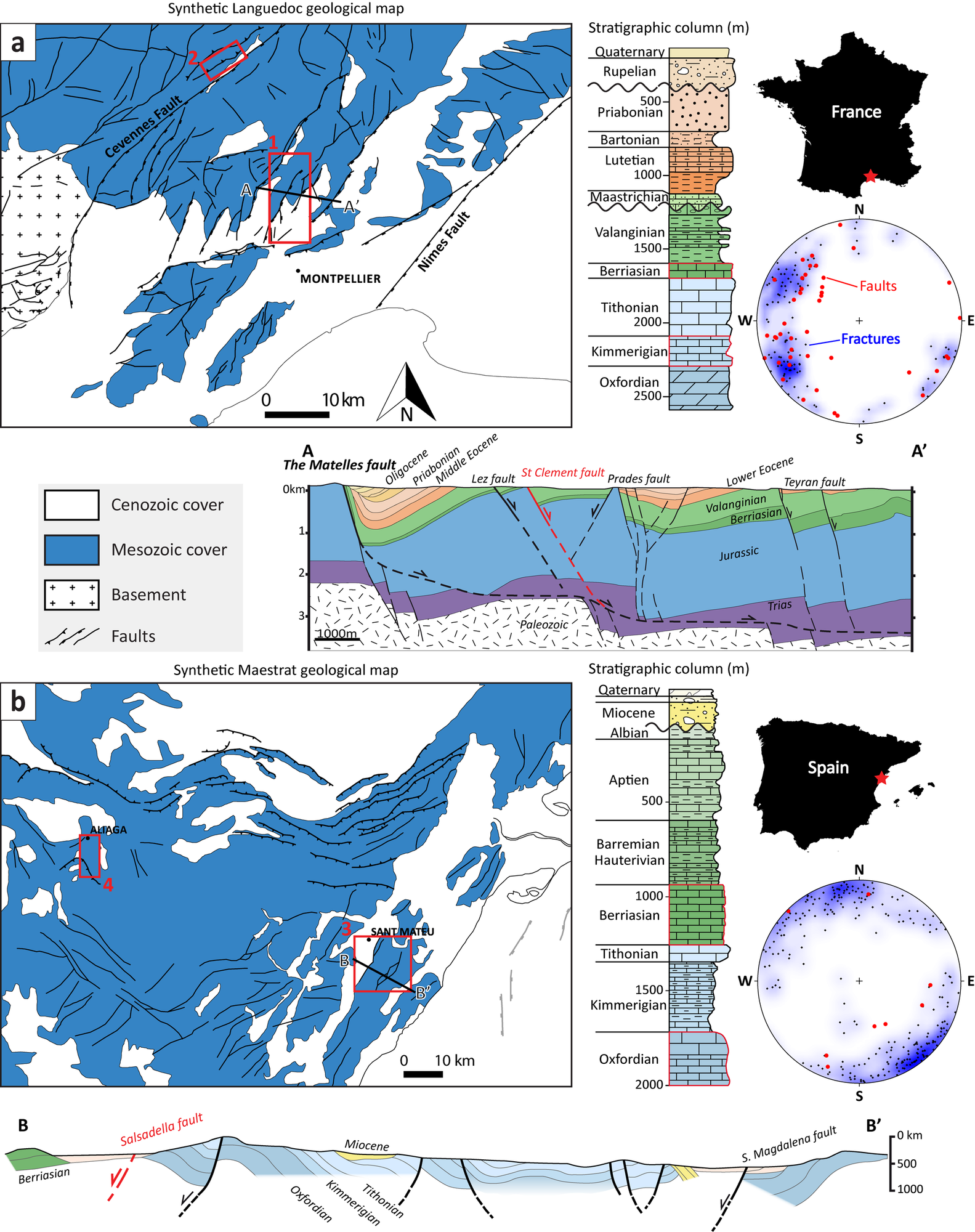
Synthetic Languedoc geological map
a
Cevennes Fault
Nimes Fault
MONTPELLIER
A
A'
1
2
0
10 km
N
Stratigraphic column (m)
Quaternary
Rupelian
500
Priabonian
Bartonian
Lutetian
1000
Maastrichian
Valanginian
1500
Berriasian
Tithonian
2000
Kimmerigian
Oxfordian
2500
France
N
W
E
S
Faults
Fractures
A
A'
The Matelles fault
Oligocene
Priabonian
Middle Eocene
Lez fault
St Clement fault
Prades fault
Lower Eocene
Teyran fault
Valanginian
Berriasian
Jurassic
Trias
Paleozoic
0km
1
2
3
1000m
Cenozoic cover
Mesozoic cover
Basement
Faults
Synthetic Maestrat geological map
b
ALTAGA
4
3
SANT MATEU
B
B'
0
10 km
Stratigraphic column (m)
Qaternary
Miocene
Albian
Aptien
500
Barremian
Hauterivian
1000
Berriasian
Tithonian
1500
Kimmerigian
Oxfordian
2000
Spain
N
W
E
S
B
B'
Salsadella fault
Berriasian
Miocene
Oxfordian
Kimmerigian
Tithonian
S. Magdalena fault
0 km
500
1000

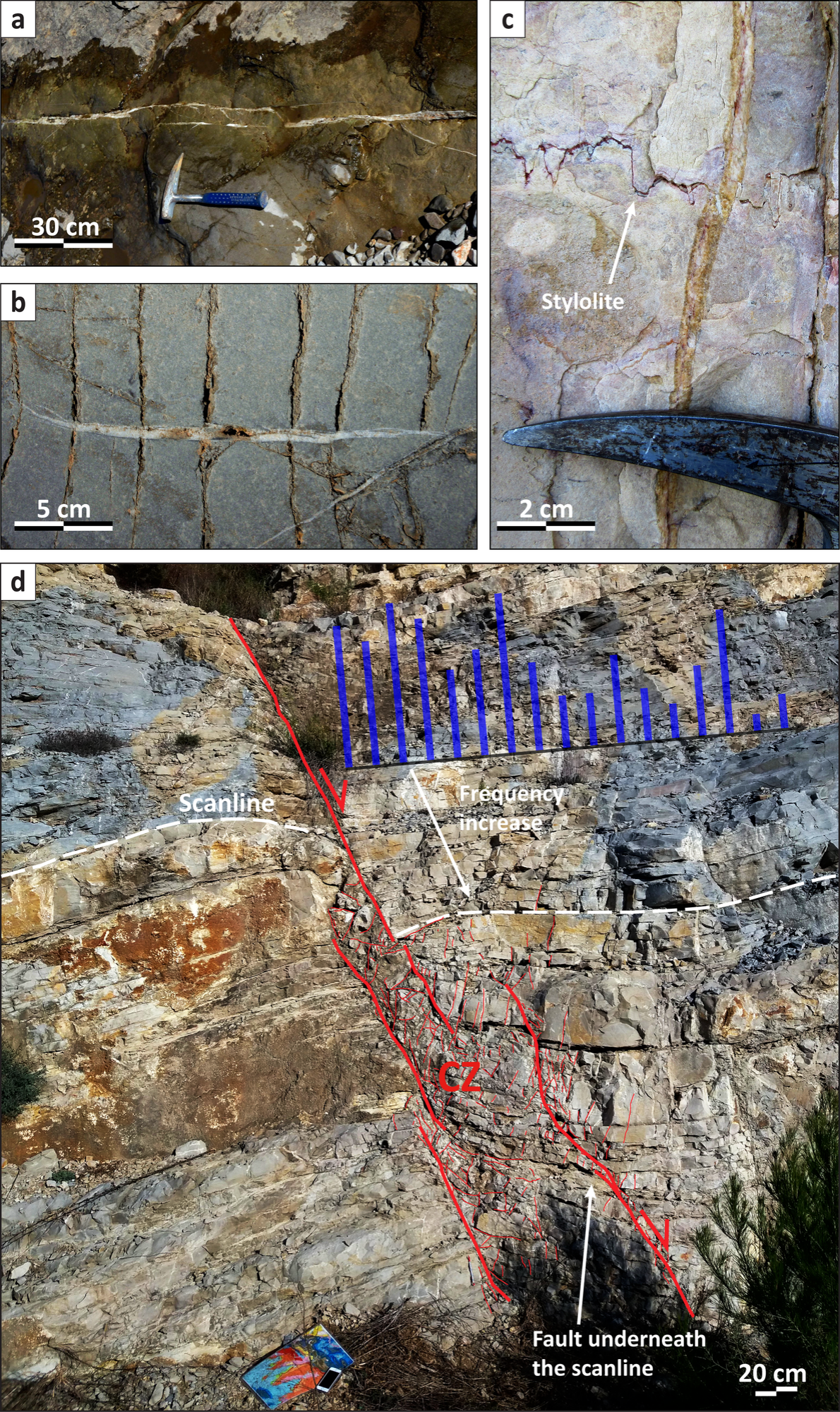
a
30 cm
b
5 cm
c
Stylolite
2 cm
d
Scanline
Frequency
increase
CZ
Fault underneath
the scanline
20 cm

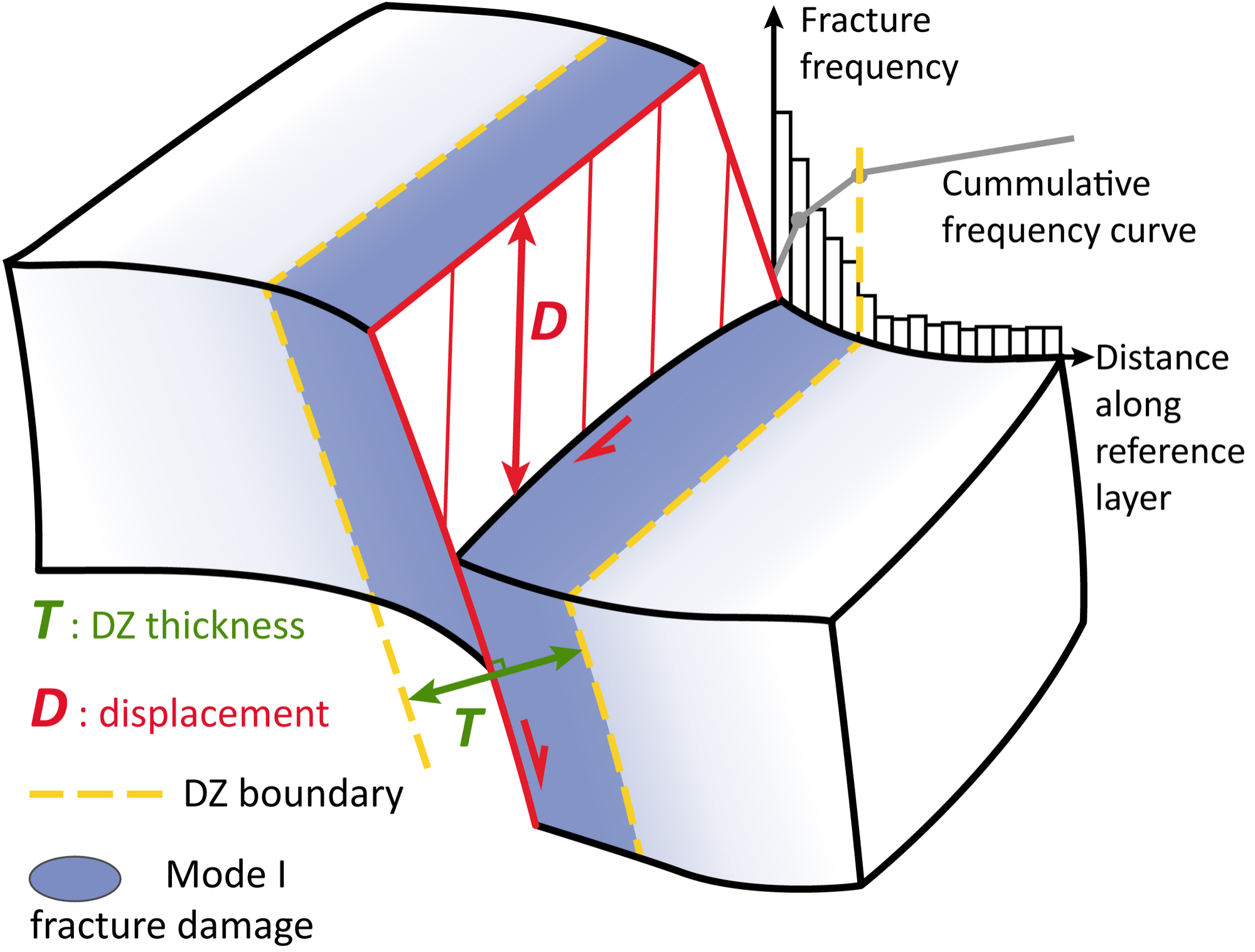
Fracture frequency
Cummulative frequency curve
Distance along reference layer
D
T
T : DZ thickness
D : displacement
DZ boundary
Mode I fracture damage

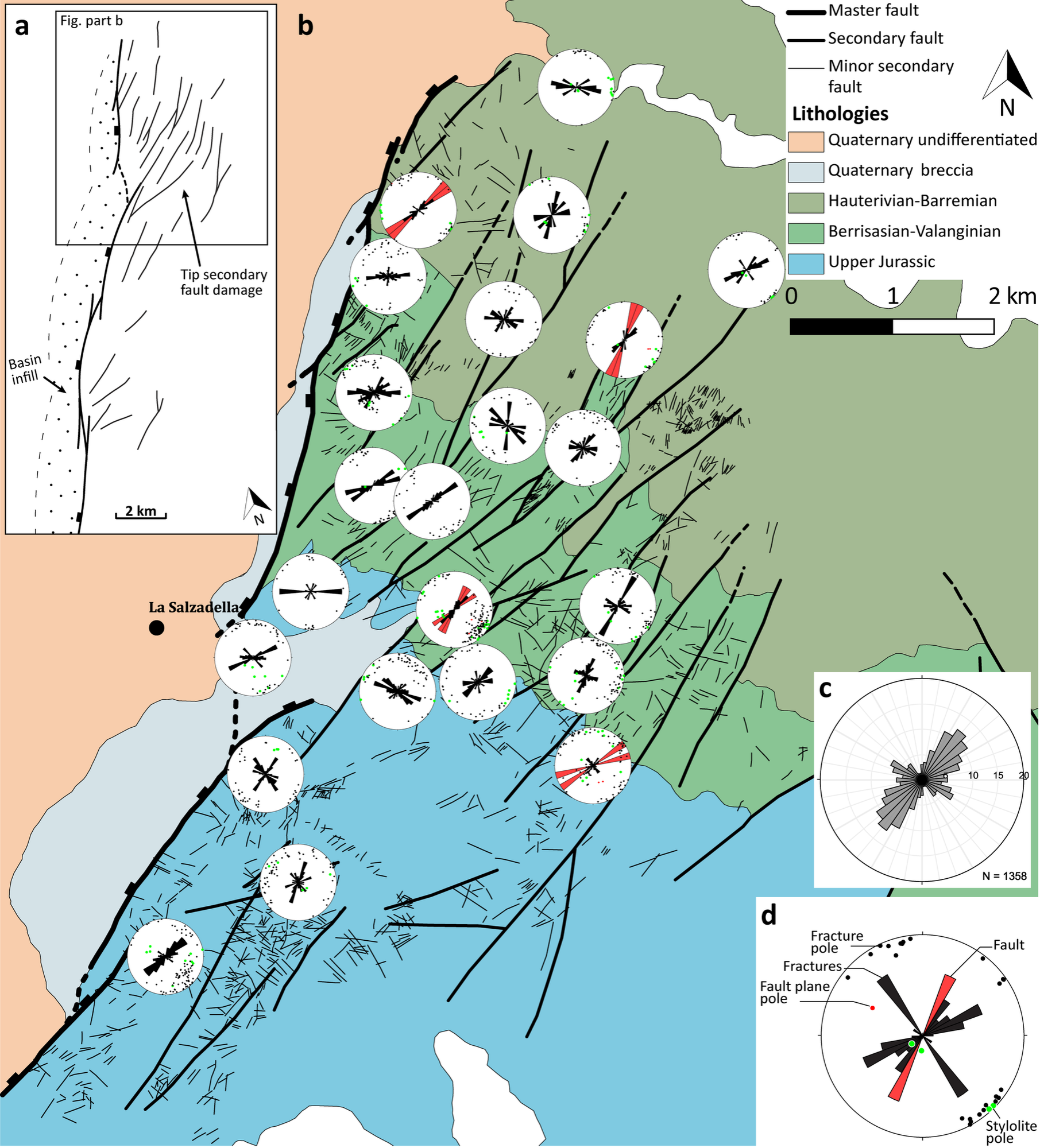
a
Fig. part b
Tip secondary fault damage
Basin infill
2 km
N
b
Master fault
Secondary fault
Minor secondary fault
N
Lithologies
Quaternary undifferentiated
Quaternary breccia
Hauterivian-Barremian
Berrisasian-Valanginian
Upper Jurassic
0
1
2 km
La Salzadella
c
10
15
20
N = 1358
d
Fracture pole
Fault
Fractures
Fault plane pole
Stylolite pole

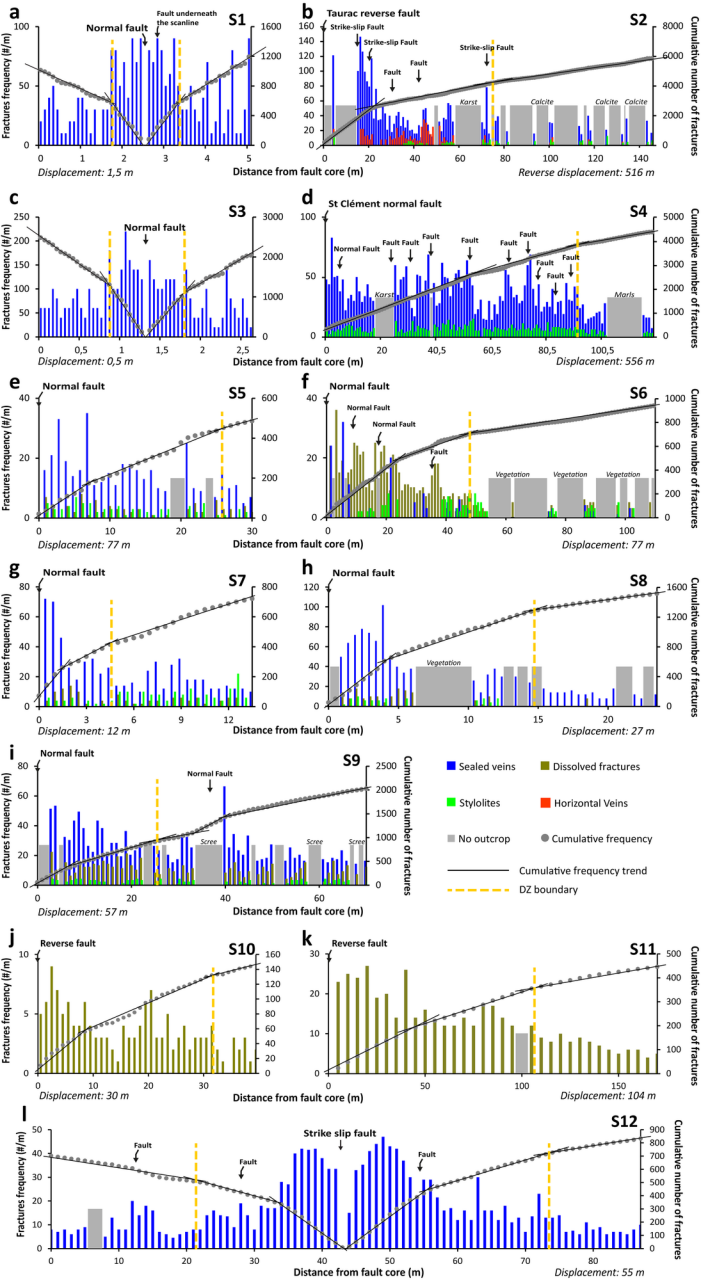
a
Normal fault
Fault underneath the scanline
S1
Fractures frequency (#/m)
Cumulative number of fractures
Displacement: 1,5 m
Distance from fault core (m)
b
Taurac reverse fault
Strike-slip Fault
Strike-slip Fault
Fault
Fault
Strike-slip Fault
Karst
Calcite
Calcite
Calcite
S2
Reverse displacement: 516 m
c
Normal fault
S3
Displacement: 0,5 m
d
St Clément normal fault
Normal Fault
Fault
Fault
Fault
Fault
Fault
Fault
Fault
Fault
Karst
Marls
S4
Displacement: 556 m
e
Normal fault
S5
Displacement: 77 m
f
Normal fault
Normal Fault
Normal Fault
Fault
Vegetation
Vegetation
Vegetation
S6
Displacement: 77 m
g
Normal fault
S7
Displacement: 12 m
h
Normal fault
Vegetation
S8
Displacement: 27 m
i
Normal fault
Normal Fault
Scree
Scree
Scree
S9
Displacement: 57 m
Sealed veins
Dissolved fractures
Stylolites
Horizontal Veins
No outcrop
Cumulative frequency
Cumulative frequency trend
DZ boundary
j
Reverse fault
S10
Displacement: 30 m
k
Reverse fault
S11
Displacement: 104 m
l
Fault
Fault
Strike slip fault
Fault
S12
Displacement: 55 m

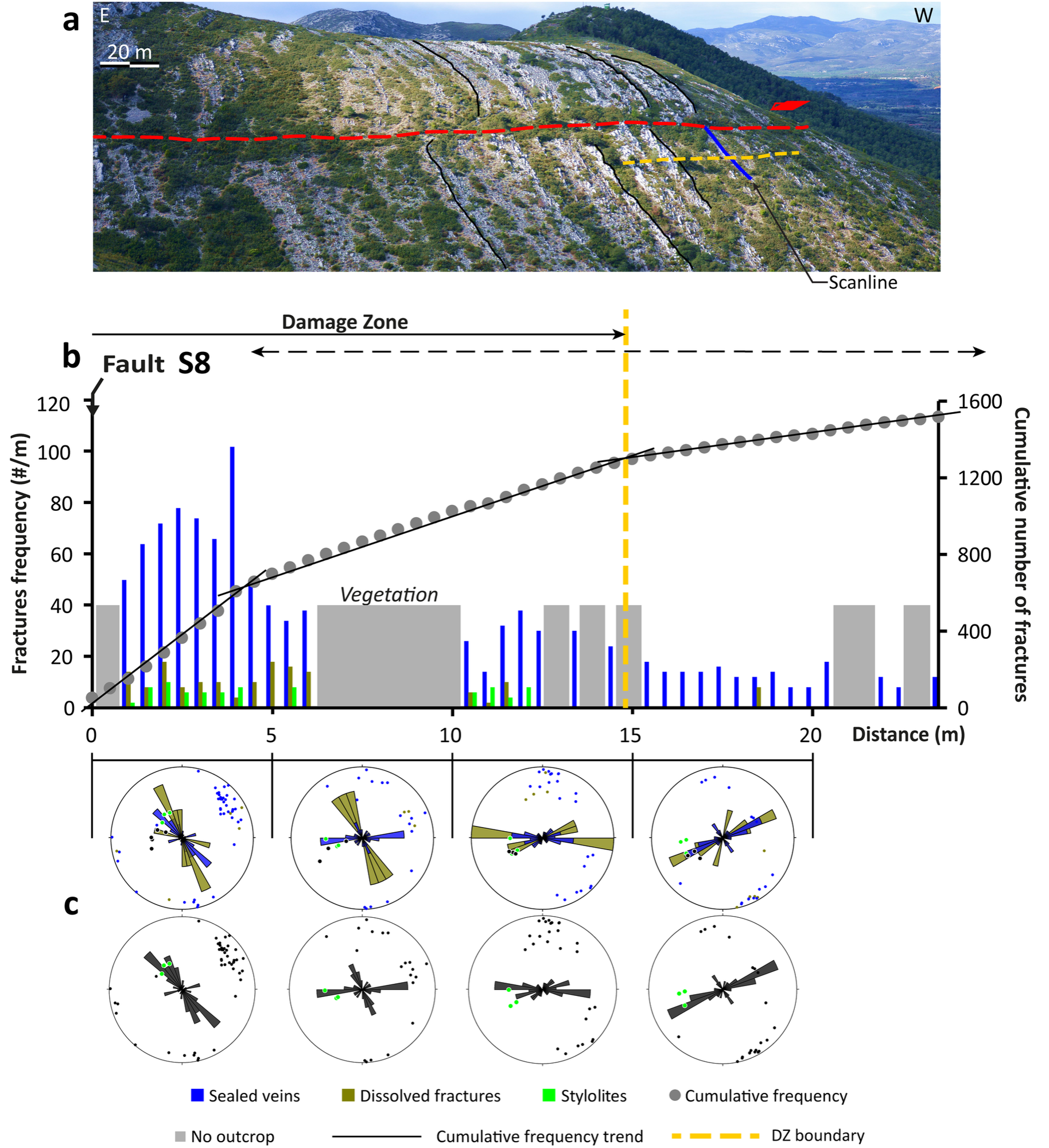
a
E
W
20 m
Scanline
Damage Zone
b
Fault S8
Fractures frequency (#/m)
Cumulative number of fractures
Vegetation
Distance (m)
0
5
10
15
20
0
20
40
60
80
100
120
0
400
800
1200
1600
c
Sealed veins
Dissolved fractures
Stylolites
Cumulative frequency
No outcrop
Cumulative frequency trend
DZ boundary

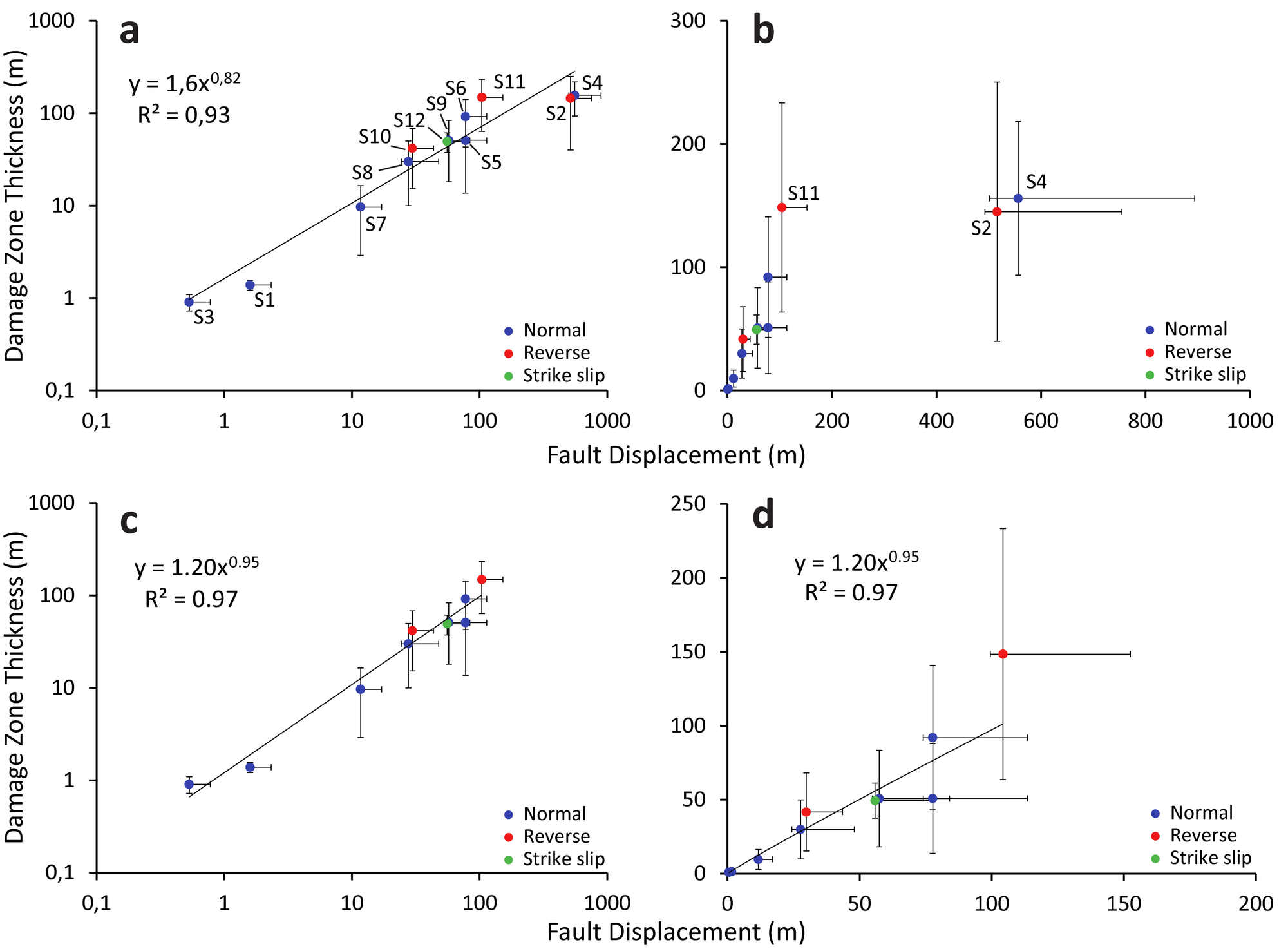
a
y = 1,6x^0,82
R² = 0,93
S1
S2
S3
S4
S5
S6
S7
S8
S9
S10
S11
S12
Normal
Reverse
Strike slip
Damage Zone Thickness (m)
1000
100
10
1
0,1
0,1
1
10
100
1000
b
300
200
100
0
0
200
400
600
800
1000
c
y = 1.20x^0.95
R² = 0.97
d
y = 1.20x^0.95
R² = 0.97
250
150
50
200
Fault Displacement (m)

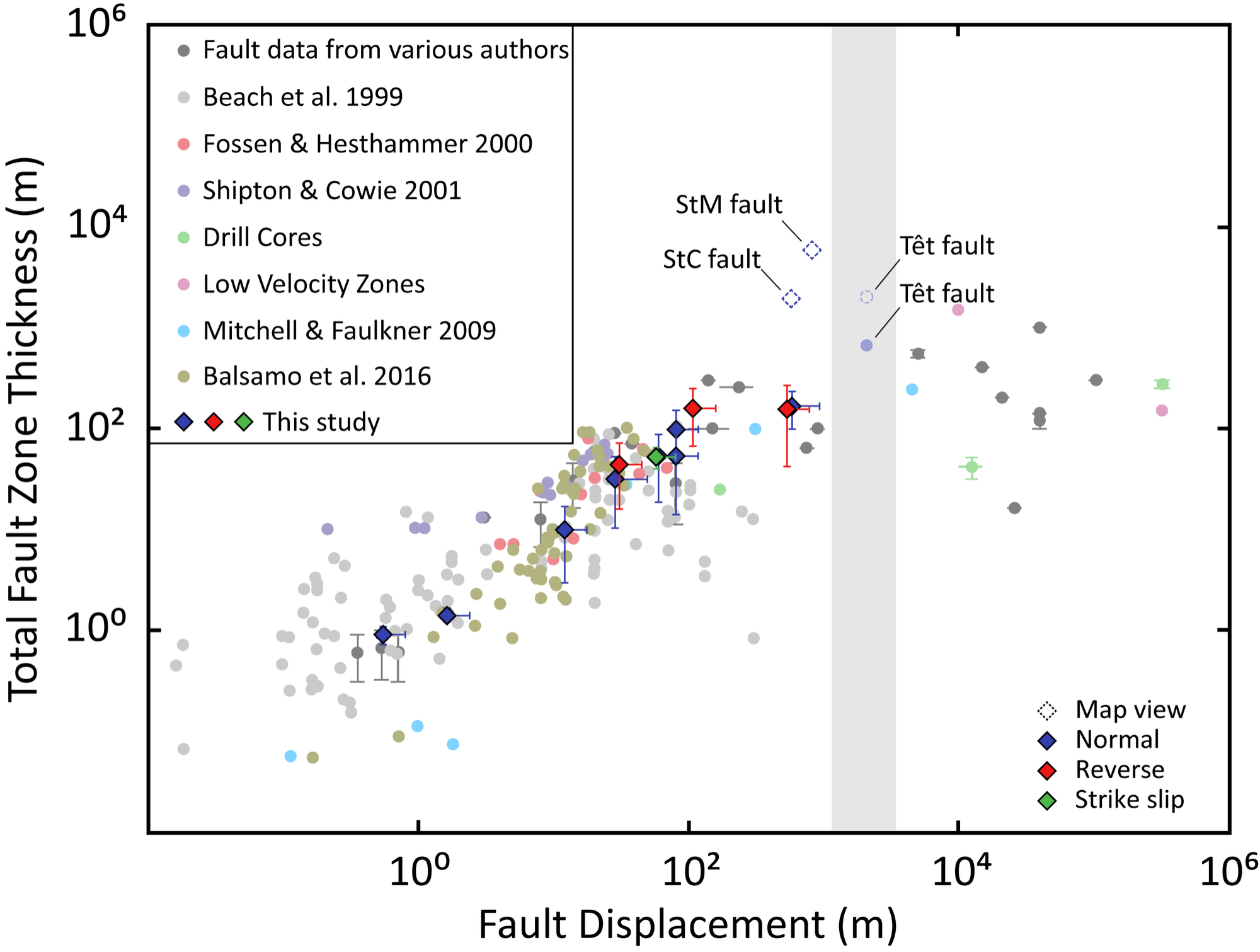
Fault data from various authors
Beach et al. 1999
Fossen & Hesthammer 2000
Shipton & Cowie 2001
Drill Cores
Low Velocity Zones
Mitchell & Faulkner 2009
Balsamo et al. 2016
This study
StM fault
StC fault
Têt fault
Têt fault
Map view
Normal
Reverse
Strike slip
Total Fault Zone Thickness (m)
Fault Displacement (m)
10⁶
10⁴
10²
10⁰
10⁰
10²
10⁴
10⁶

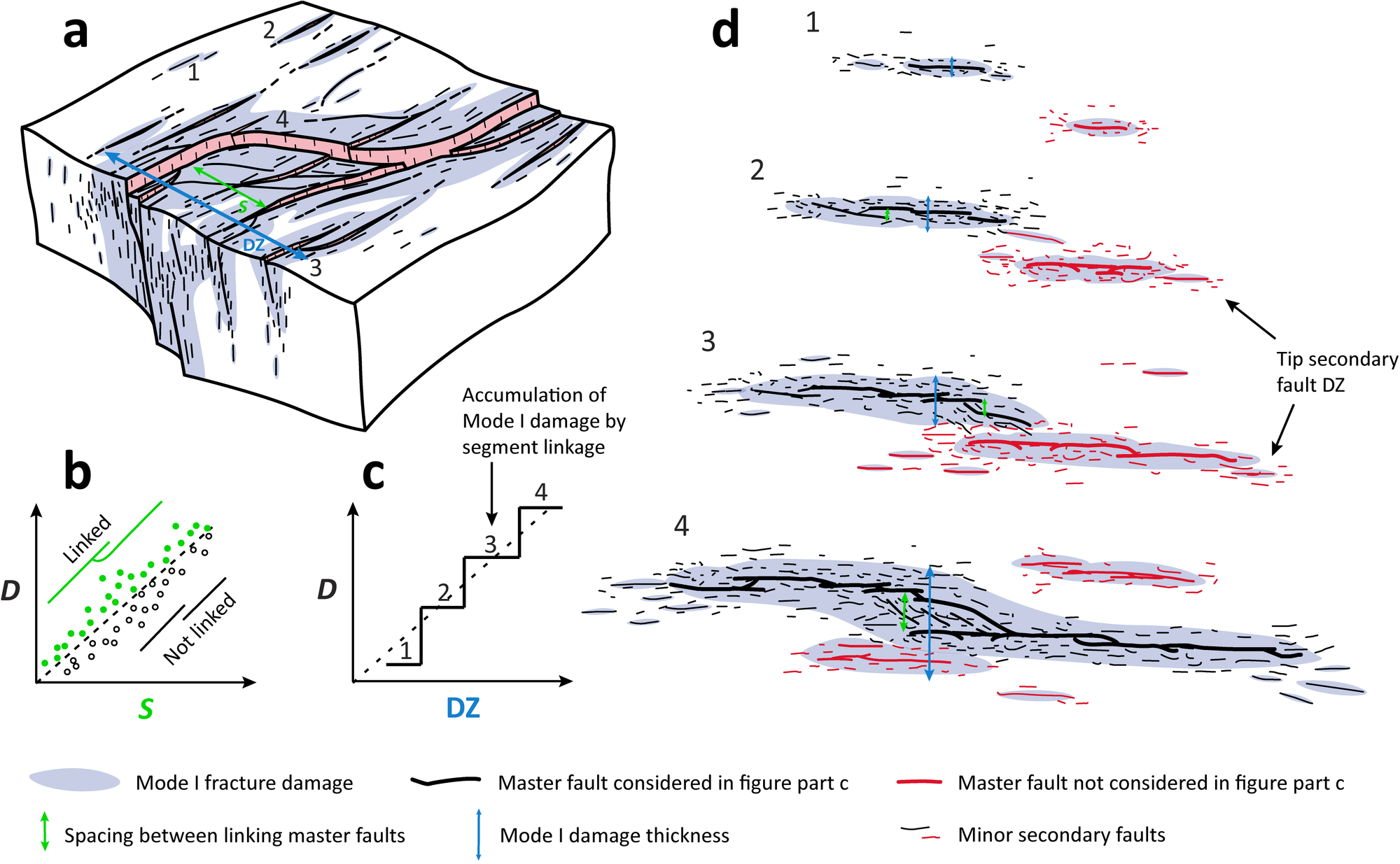
a
1
2
3
4
S
DZ
b
Linked
Not linked
D
S
c
Accumulation of
Mode I damage by
segment linkage
D
DZ
d
Tip secondary
fault DZ
Mode I fracture damage
Master fault considered in figure part c
Master fault not considered in figure part c
Spacing between linking master faults
Mode I damage thickness
Minor secondary faults

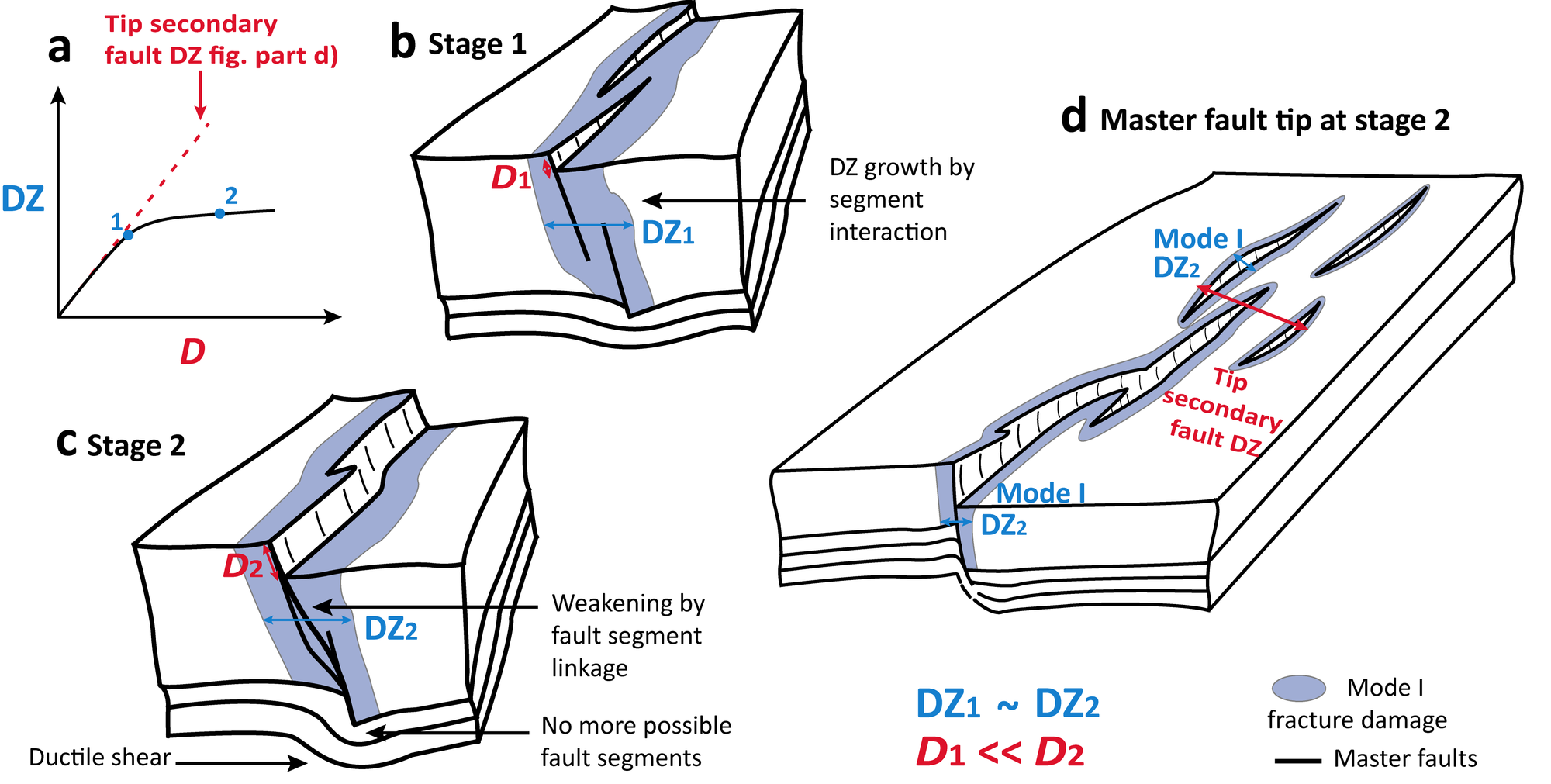
a
Tip secondary fault DZ fig. part d)
DZ
D
1
2
b Stage 1
D1
DZ1
DZ growth by segment interaction
c Stage 2
D2
DZ2
Weakening by fault segment linkage
No more possible fault segments
Ductile shear
d Master fault tip at stage 2
Mode I
DZ2
Tip secondary fault DZ
Mode I
DZ2
DZ1 ~ DZ2
D1 << D2
Mode I fracture damage
Master faults